METHODS

Specimens. Primary tumour specimens were obtained from patients who were diagnosed with DLBCL, follicular lymphoma, MCL, MALT lymphoma, or classical Hodgkin's lymphoma. In total, 238 primary lymphoma specimens listed in Supplementary Table 1 were subjected to SNP array analysis. Three Hodgkin's-lymphoma-derived cell lines (KM-H2, HDLM2, L540) were obtained from Hayashibara Biochemical Laboratories, Inc., Fujisaki Cell Center and were also analysed by SNP array analysis.

Microarray analysis. High-molecular-mass DNA was isolated from tumour specimens and subjected to SNP array analysis using GeneChip Mapping 50K and/or 250K arrays (Affymetrix). The scanned array images were processed with Gene Chip Operation software (GCOS), followed by SNP calls using GTYPE. Genome-wide copy number measurements and LOH detection were performed using CNAG/AsCNAR software[12,13].

Mutation analysis. Mutations in the *A20* gene were examined in 265 samples of B-lineage lymphoma, including 62 DLBCLs, 52 follicular lymphomas, 87 MALTs, 37 MCLs and 3 Hodgkin's-lymphoma-derived cell lines and 24 primary Hodgkin's lymphoma samples, by direct sequencing using an ABI PRISM 3130xl Genetic Analyser (Applied Biosystems). To analyse primary Hodgkin's lymphoma samples in which CD30-positive tumour cells (Reed–Sternberg cells) account for only a fraction of the specimen, 150 Reed–Sternberg cells were collected for each 10 μm slice of a formalin-fixed block immunostained for CD30 by laser-capture microdissection (ASLMD6000, Leica), followed by genomic DNA extraction using QIAamp DNA Micro kit (Qiagen). The primer sets used in this study are listed in Supplementary Table 6.

Functional analysis of wild-type and mutant A20. Full-length cDNA for wild-type *A20* was isolated from total RNA extracted from an acute myeloid leukaemia-derived cell line, CTS, and subcloned into a lentivirus vector (pLenti4/TO/V5-DEST, Invitrogen). cDNAs for mutant A20 were generated by PCR amplification using mutagenic primers (Supplementary Table 6), and introduced into the same lentivirus vector. Forty-eight hours after transfection of each plasmid into 293FT cells using the calcium phosphate method, lentivirus stocks were obtained from ultrafiltration using Amicon Ultra (Millipore), and used to infect KM-H2 cells to generate stable transfectants of mock, wild-type and mutant A20. Each KM-H2 derivative cell line was further transduced stably with a reporter plasmid (pGL4.32, Promega) containing a luciferase gene under an NF-κB-responsive element by electroporation using Nucleofector reagents (Amaxa).

Assays for cell proliferation and NF-κB activity. Proliferation of the KM-H2 derivative cell lines was assayed in triplicate using a Cell Counting Kit (Dojindo). The mean absorption of five independent assays was plotted with s.d. for each derivative line. Two independent KM-H2-derived cell lines were used for each experiment. The NF-κB activity in KM-H2 derivatives for A20 mutants was evaluated by luciferase assays using a PiccaGene Luciferase Assay Kit (TOYO B-Net Co.). Each assay was performed in triplicate and the mean absorption of five independent experiments was plotted with s.d.

Western blot analyses. Polyclonal anti-sera against N-terminal (anti-A20N) and C-terminal (anti-A20C) A20 peptides were generated by immunizing rabbits with these peptides (LSNMRKAVKIRERTPEDIC for anti-A20N and CFQFKQMYG for anti-A20C, respectively). Total cell lysates from KM-H2 cells were separated on 7.5% polyacrylamide gel and subjected to western blot analysis using antibodies to A20 (anti-A20N and anti-A20C), IκBα (sc-847), IκBβ (sc-945), IκBγ (sc-7155) and actin (sc-8432) (Santa Cruz Biotechnology).

Functional analyses of wild-type and mutant A20. Each KM-H2 derivative cell line stably transduced with various *Tet*-inducible A20 constructs was cultured in serum-free medium in the presence or absence of A20 induction using 1 μg ml^{-1} of tetracycline, and cell number was counted every day. 1×10^6 cells of each KM-H2 derivative cell line were analysed for their intracellular levels of IκBβ and IκBε and for NF-κB activities by western blot analyses and luciferase assays, respectively, 12 h after the beginning of cell culture. Effects of human recombinant TNF-α and lymphotoxin-α (210-TA and 211-TB, respectively, R&D Systems) on the NF-κB pathway and cell proliferation were evaluated by adding both cytokines into 10 ml of serum-free cell culture at a concentration of 200 pg ml^{-1}. For cell proliferation assays, culture medium was half replaced every 12 h to minimize the side-effects of autocrine cytokines. Intracellular levels of IκBβ, IκBε and NF-κB were examined 12 h after the beginning of the cell culture. To evaluate the effect of neutralizing TNF-α and lymphotoxin-α, 1×10^6 of KM-H2 cells transduced with both *Tet*-inducible A20 and the NF-κB-luciferase reporter were pre-cultured in serum-free media for 36 h, and thereafter neutralizing antibodies against TNF-α (MAB210, R&D Systems) and/or lymphotoxin-α (AF-211-NA, R&D Systems) were added to the media at a concentration of 200 pg ml^{-1}. After the extended culture during 12 h with or without 1 μg ml^{-1} tetracycline, the intracellular levels of IκBβ and IκBε and NF-κB activities were examined by western blot analysis and luciferase assays, respectively. To examine the effects of A20 re-expression on apoptosis, 1×10^6 KM-H2 cells were cultured for 4 days in 10 ml medium with or without *Tet* induction. After staining with phycoerythrin-conjugated anti-Annexin-V (ID556422, Becton Dickinson), Annexin-V-positive cells were counted by flow cytometry at the indicated times.

***In vivo* tumorigenicity assays.** KM-H2 cells transduced with a mock or *Tet*-inducible wild-type *A20* gene were inoculated into NOG mice and their tumorigenicity was examined for 5 weeks with or without tetracycline administration. Injections of 7×10^6 cells of each KM-H2 cell line were administered to two opposite sites in four mice. Tetracycline was administered in drinking water at a concentration of 200 μg ml^{-1}.

ELISA. Concentrations of TNF-α, lymphotoxin-α, IL-1, IL-2, IL-4, IL-6, IL-12, IL-18 and TGF-β in the culture medium were measured after 48 h using ELISA. For those cytokines detectable after 48-h culture (TNFα, LTα, and IL-6), their time course was examined further using the Quantikine ELISA kit (R&D Systems).

Statistical analysis. Significance of the difference in NF-κB activity between two given groups was evaluated using a paired *t*-test, in which the data from each independent luciferase assay were paired to calculate test statistics. To evaluate the effect of A20 re-expression in KM-H2 cells on apoptosis, the difference in the fractions of Annexin-V-positive cells between Tet (+) and Tet (−) groups was also tested by a paired *t*-test for assays, in which the data from the assays performed on the same day were paired.

©2009 Macmillan Publishers Limited. All rights reserved

nature

Vol 460|13 August 2009|doi:10.1038/nature08240

LETTERS

Gain-of-function of mutated *C-CBL* tumour suppressor in myeloid neoplasms

Masashi Sanada[1,5]*, Takahiro Suzuki[7]*, Lee-Yung Shih[8]*, Makoto Otsu[9], Motohiro Kato[1,2], Satoshi Yamazaki[6], Azusa Tamura[1], Hiroaki Honda[11], Mamiko Sakata-Yanagimoto[12], Keiki Kumano[3], Hideaki Oda[13], Tetsuya Yamagata[14], Junko Takita[1,2,3], Noriko Gotoh[10], Kumi Nakazaki[1,4], Norihiko Kawamata[15], Masafumi Onodera[16], Masaharu Nobuyoshi[7], Yasuhide Hayashi[17], Hiroshi Harada[18], Mineo Kurokawa[3,4], Shigeru Chiba[12], Hiraku Mori[18], Keiya Ozawa[7], Mitsuhiro Omine[18], Hisamaru Hirai[3,4], Hiromitsu Nakauchi[6,9], H. Phillip Koeffler[15] & Seishi Ogawa[1,5]

Acquired uniparental disomy (aUPD) is a common feature of cancer genomes, leading to loss of heterozygosity. aUPD is associated not only with loss-of-function mutations of tumour suppressor genes[1], but also with gain-of-function mutations of proto-oncogenes[2]. Here we show unique gain-of-function mutations of the *C-CBL* (also known as *CBL*) tumour suppressor that are tightly associated with aUPD of the 11q arm in myeloid neoplasms showing myeloproliferative features. The *C-CBL* proto-oncogene, a cellular homologue of *v-Cbl*, encodes an E3 ubiquitin ligase and negatively regulates signal transduction of tyrosine kinases[3–6]. Homozygous *C-CBL* mutations were found in most 11q-aUPD-positive myeloid malignancies. Although the *C-CBL* mutations were oncogenic in NIH3T3 cells, c-Cbl was shown to functionally and genetically act as a tumour suppressor. C-CBL mutants did not have E3 ubiquitin ligase activity, but inhibited that of wild-type C-CBL and CBL-B (also known as CBLB), leading to prolonged activation of tyrosine kinases after cytokine stimulation. *c-Cbl*$^{-/-}$ haematopoietic stem/progenitor cells (HSPCs) showed enhanced sensitivity to a variety of cytokines compared to *c-Cbl*$^{+/+}$ HSPCs, and transduction of *C-CBL* mutants into *c-Cbl*$^{-/-}$ HSPCs further augmented their sensitivities to a broader spectrum of cytokines, including stem-cell factor (SCF, also known as KITLG), thrombopoietin (TPO, also known as THPO), IL3 and FLT3 ligand (FLT3LG), indicating the presence of a gain-of-function that could not be attributed to a simple loss-of-function. The gain-of-function effects of C-CBL mutants on cytokine sensitivity of HSPCs largely disappeared in a *c-Cbl*$^{+/+}$ background or by co-transduction of wild-type *C-CBL*, which suggests the pathogenic importance of loss of wild-type *C-CBL* alleles found in most cases of *C-CBL*-mutated myeloid neoplasms. Our findings provide a new insight into a role of gain-of-function mutations of a tumour suppressor associated with aUPD in the pathogenesis of some myeloid cancer subsets.

Myelodysplastic syndromes (MDS) are heterogeneous groups of blood cancers originating from haematopoietic precursors. They are characterized by deregulated haematopoiesis showing a high propensity to acute myeloid leukaemia (AML)[7]. Some MDS cases have overlapping clinico-pathological features with myeloproliferative disorders, and are now classified into myelodysplasia/myeloproliferative neoplasms (MDS/MPN) by the World Health Organization (WHO) classification[8]. To obtain a comprehensive profile of allelic imbalances in these myeloid neoplasms, we performed allele-specific copy number analyses of bone marrow samples obtained from 222 patients with MDS, MDS/MPN, or other related myeloid neoplasms (Supplementary Tables 1 and 2) using high-density single nucleotide polymorphism (SNP) arrays combined with CNAG/AsCNAR software[9,10].

Genomic profiles of MDS and MDS/MPN showed characteristic unbalanced genetic changes, as reported in previous cytogenetic studies[11] (Supplementary Fig. 1a); however, they were detected more sensitively by SNP array analyses (Supplementary Table 3). aUPD was detected in 70 samples (31.5%) on the basis of the allele-specific copy number analyses, which substantially exceeded the detection rate obtained using a SNP call-based detection algorithm (20.7%) (Supplementary Figs 2 and 4, and Supplementary Tables 4 and 5). Long stretches of homozygous SNP calls caused by shared identical-by-descent alleles in parents were empirically predicted and excluded (Supplementary Fig. 3). aUPDs were more common in MDS/MPN than in MDS. They preferentially affected several chromosomal arms (1p, 1q, 4q, 7q, 11p, 11q, 14q, 17p and 21q) in distinct subsets of patients, and frequently associated with mutated oncogenes and tumour suppressor genes (Supplementary Figs 1b and 5). Among these, the most common aUPDs were those involving 11q ($n = 17$), which defined a unique subset of myeloid neoplasms that were clinically characterized by frequent diagnosis of chronic myelomonocytic leukaemia (CMML) with normal karyotypes (13 cases) (Fig. 1a and Supplementary Table 6). We identified a minimum overlapping aUPD segment of approximately 1.4 megabases (Mb) in 11q, which contained a mutated *C-CBL* proto-oncogene (Fig. 1b).

[1]Cancer Genomics Project, [2]Department of Pediatrics, [3]Cell Therapy and Transplantation Medicine, and [4]Hematology and Oncology, Graduate School of Medicine, The University of Tokyo, 7-3-1 Hongo, Bunkyo-ku, Tokyo 113-8655, Japan. [5]Core Research for Evolutional Science and Technology, [6]Exploratory Research for Advanced Technology, Japan Science and Technology Agency, 4-1-8 Honcho, Kawaguchi-shi, Saitama 332-0012, Japan. [7]Division of Hematology, Department of Medicine, Jichi Medical University, 3311-1 Yakushiji, Shimotsuke-shi, Tochigi 329-0498, Japan. [8]Division of Hematology-Oncology, Department of Internal Medicine, Chang Gung Memorial Hospital, Chang Gung University, 199 Tung Hwa North Road, Taipei 105, Taiwan. [9]Division of Stem Cell Therapy, Center for Stem Cell and Regenerative Medicine, [10]Division of Systems Biomedical Technology, Institute of Medical Science, The University of Tokyo, 4-6-1 Shirokanedai, Minato-ku, Tokyo 108-8639, Japan. [11]Department of Developmental Biology, Research Institute of Radiation Biology and Medicine, Hiroshima University, 1-2-3 Kasumi, Minami-ku, Hiroshima 734-8553, Japan. [12]Department of Clinical and Experimental Hematology, Institute of Clinical Medicine, University of Tsukuba, 1-1-1 Tennodai, Tukuba-shi, Ibaraki, 305-8571, Japan. [13]Department of Pathology, Tokyo Women's Medical University, 8-1 Kawada-cho, Shinjuku-ku, Tokyo 162-8666, Japan. [14]Department of Hematology, Dokkyo University School of Medicine, 800 Kitabayashi, Mibu, Tochigi 321-0293, Japan. [15]Hematology/Oncology, Cedars-Sinai Medical Center, 8700 Beverly Boulevard, Los Angeles, California 90048, USA. [16]Department of Genetics, National Research Institute for Child Health and Development, 2-10-1 Okura, Setagaya-ku, Tokyo, 157-8535, Japan. [17]Gunma Children's Medical Center, 779 Shimohakoda, Hokkitsu-machi, Shibukawa-shi, Gunma 377-8577, Japan. [18]Division of Hematology, Internal Medicine, Showa University Fujigaoka Hospital, 1-30 Fujigaoka, Aoba-ku, Yokohama, Kanagawa 227-8501, Japan.
*These authors contributed equally to this work.

©2009 Macmillan Publishers Limited. All rights reserved

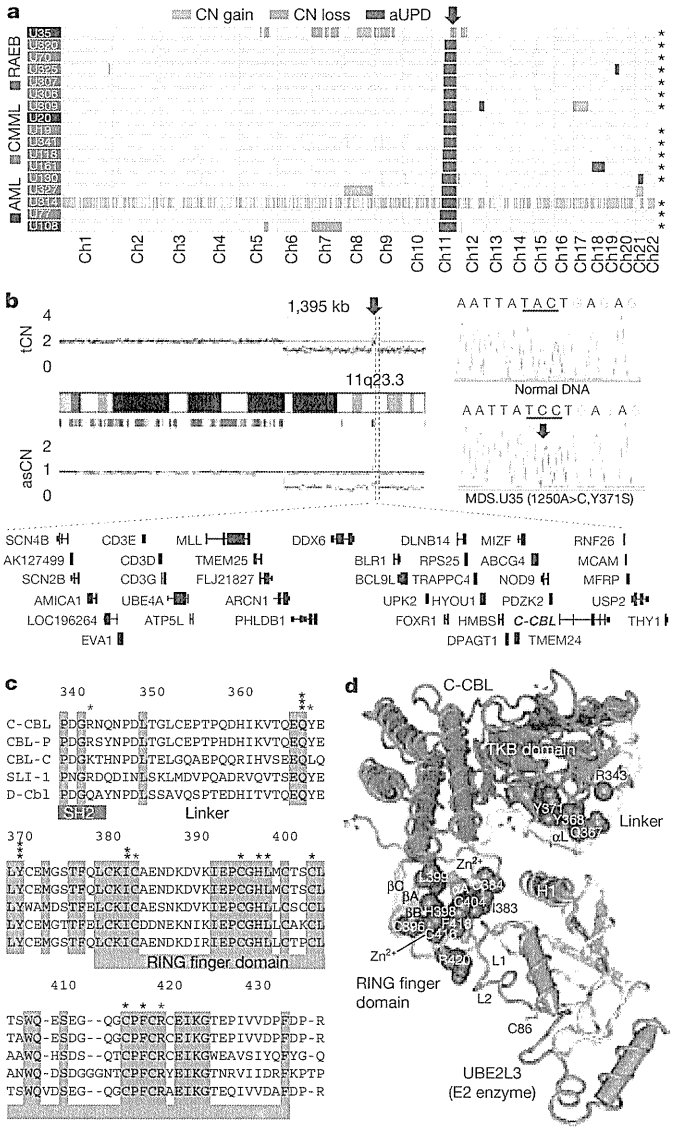

Figure 1 | Common UPD on the 11q arm and *C-CBL* mutations in myeloid neoplasms. a, Copy number profiles of 17 cases with myeloid neoplasms showing 11qUPD. Regions of copy number (CN) gains, losses and aUPD are depicted in different colours. Histologies are shown by coloured boxes. Asterisks denote *C-CBL*-mutated cases. Ch, chromosome; RAEB, refractory anaemia with excess blasts. **b**, CNAG output for MDS.U35. Total copy number (tCN) and allele-specific copy number (asCN) plots show a focal copy number gain spanning a 1.4-Mb segment within 3 Mb of an 11q-aUPD region (left), which contained mutated *C-CBL* in MDS.U35 (right). **c**, Alignments of amino acid sequences for human CBL family proteins and their homologues in *Caenorhabditis elegans* (SLI-1) and *Drosophila* (D-Cbl). Amino acid numbering is on the basis of human *C-CBL*. Conserved amino acids are highlighted. Positions of mutated amino acids are indicated by asterisks. Heterozygous mutations are shown in red. **d**, Mutated amino acid positions in the three-dimensional structure of a human C-CBL–UBE2L3 complex. TKB, tyrosine kinase binding domain.

C-CBL is the cellular homologue of the *v-Cbl* transforming gene of the Cas NS-1 murine leukaemia virus[5,12]. It was recently found to be mutated in human AML cases[13–15]. Together with its close homologue, CBL-B, C-CBL is thought to be involved in the negative modulation of tyrosine kinase signalling, primarily through their E3 ubiquitin ligase activity that is responsible for the downregulation of activated tyrosine kinases[3–5]. By sequencing all *C-CBL* exons in all 222 samples, we found *C-CBL* mutations in 15 of the 17 cases with 11q-aUPD, whereas only 3 out of 205 cases without 11q-aUPD had *C-CBL* mutations, showing a strong association of *C-CBL* mutations with 11q-aUPD ($P = 1.46 \times 10^{-18}$) (Supplementary Fig. 6 and Supplementary Tables 6 and 7), as also indicated in a recent report[16]. Thus, *C-CBL* was thought to be the major, if not the only, target of 11q-aUPD in myeloid neoplasms. Two different *C-CBL* mutations co-existed in three cases (Supplementary Fig. 6b). Somatic origins of the mutations were confirmed in three evaluable cases (Supplementary Fig. 6c).

In most cases, *C-CBL* mutations were missense, involving the evolutionarily conserved amino acids within the linker-RING finger domain that is central to the E3 ubiquitin ligase activity[17] (Fig. 1c). Another case with a predominant Cys384Tyr mutation also contained a nonsense mutation (Arg343X) in a minor subclone, which resulted in a v-Cbl-like truncated protein (Supplementary Fig. 6b). In the remaining two cases, mutations led to amino acid deletions (Δ369−371 and Δ368−382) involving the highly conserved α-helix (αL) of the linker domain and the first loop of the RING finger. According to the published crystal structure of *C-CBL*[17], most of the mutated or deleted amino acids were positioned on the interface for the binding to the E2 enzyme (Fig. 1d), making contact with either the tyrosine kinase binding domain (Tyr 368 and Tyr 371) or E2 ubiquitin-conjugating enzymes (Ile 383, Cys 404 and Phe 418). Especially, all seven linker-domain mutations selectively involved just three amino acids (Gln 367, Tyr 368 and Tyr 371) within the conserved αL helix (Fig. 1d). Mutations were clearly homozygous in nine cases, and the apparently heterozygous chromatograms in the other six cases could also be compatible with homozygous mutations affecting the aUPD-positive tumour clones, given the presence of substantial normal cell components within these samples. Mutations in the remaining three cases were considered to be heterozygous. About half of the *C-CBL*-mutated cases carried coexisting mutations of *RUNX1* (four cases), *TP53* (one case), *FLT3* internal tandem duplication (1 case) or *JAK2* (3 cases). *NRAS* and *KRAS* mutations were prevalent among CMML (15.1%) but occurred within discrete clusters from *C-CBL*-mutated cases (Supplementary Tables 2 and 6 and Supplementary Fig. 5). The mutation status of *C-CBL* did not substantially affect the clinical outcome (Supplementary Fig. 7).

All tested *C-CBL* mutants induced clear oncogenic phenotypes in NIH3T3 fibroblasts, as demonstrated by enhanced colony formation in soft agar and tumour generation in nude mice (Supplementary Fig. 8). Transformed NIH3T3 cells showed PI3 kinase-dependent activation of Akt and the transformed phenotype was reverted by treatment with the PI3 kinase inhibitor Ly294002 (Supplementary Fig. 9). When introduced into $Lin^{-}Sca1^{+}c\text{-}Kit^{+}$ (LSK) HSPCs, C-CBL mutants (C-CBL(Gln367Pro) and C-CBL(Tyr371Ser)), as well as a mouse lymphoma-derived oncogenic mutant (C-CBL(70Z)), significantly promoted the replating capacity of these progenitors (Fig. 2a). Because c-Cbl negatively modulates tyrosine kinase signalling, and all *C-CBL* mutations, including those previously reported[13–16], affected the critical domains for its enzymatic activity involved in this modulation, C-CBL was postulated to have a tumour suppressor function; loss-of-function could be a mechanism for the oncogenicity of these C-CBL mutants[3,5]. To assess this possibility and to clarify further the role of *C-CBL* mutations in the pathogenesis of myeloid neoplasms, we generated $c\text{-}Cbl^{-/-}$ mice and examined their haematological phenotypes (Supplementary Fig. 10).

In agreement with previous reports[18–20], $c\text{-}Cbl^{-/-}$ mice exhibited splenomegaly and an augmented haematopoietic progenitor pool, as was evident from the increased colony formation of bone marrow cells in methylcellulose culture and higher numbers of LSK and CD34-negative LSK cells in bone marrow and/or spleen compared to their wild-type littermates (Fig. 2b–d and Supplementary Fig. 11). Furthermore, when introduced into a *BCR-ABL* transgenic background[21], the $c\text{-}Cbl^{-/-}$ allele accelerated blastic crisis depending on the allele dosage (Fig. 2e, f). These observations supported the notion that wild-type *C-CBL* has tumour suppressor functions, whereas 'mutant' *C-CBL* acts as an oncogene; *C-CBL* can therefore be both a proto-oncogene and a tumour suppressor gene.

©2009 Macmillan Publishers Limited. All rights reserved

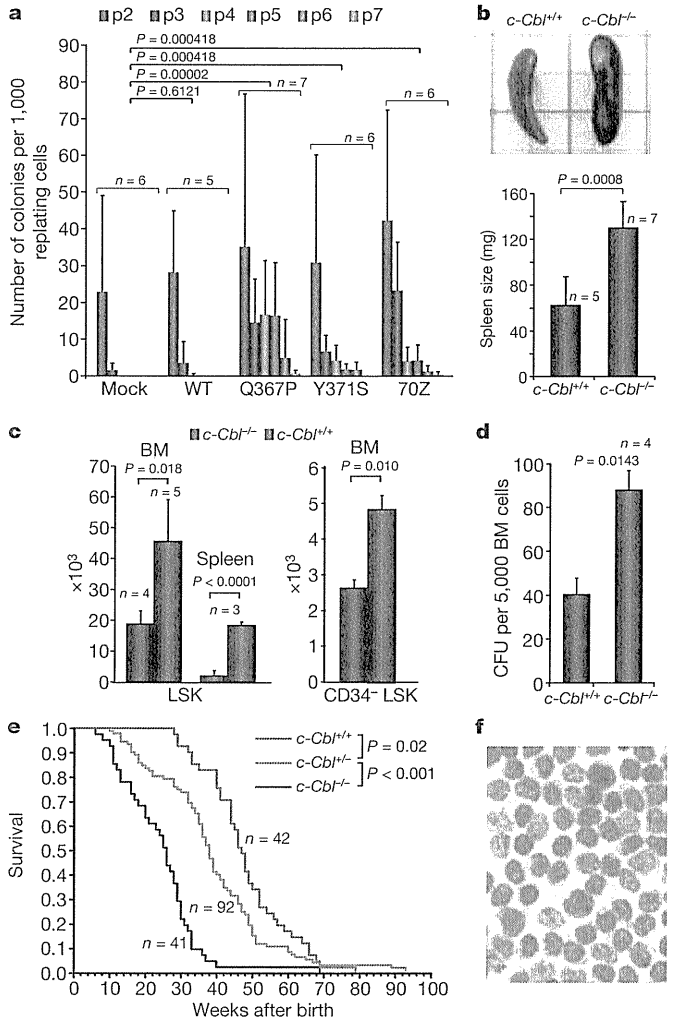

Figure 2 | Tumour-suppressor functions of wild-type C-CBL. **a**, Prolonged replating capacity of LSK cells transduced with mutant *C-CBL* (*C-CBL*(Gln367Pro) and *C-CBL*(Tyr371Ser)), compared to mock- or wild-type *C-CBL*-transduced cells. Replating capacity in methylcellulose culture is shown as mean colony number (and s.d.) per 1,000 replating cells at indicated times of replating. p, passage. **b**, Increased spleen mass in *c-Cbl*$^{-/-}$ mice compared to *c-Cbl*$^{+/+}$ mice (mean spleen weight and s.d.). **c**, Mean number of total LSK (left) and CD34-negative LSK (right) cells (plus s.d.) in bone marrow (BM) and/or spleen in *c-Cbl*$^{+/+}$ (blue columns) and *c-Cbl*$^{-/-}$ mice (red columns). Bone marrow cells from bilateral tibias and femurs were counted for each mouse. **d**, Augmented colony-forming potential of bone marrow cells from *c-Cbl*$^{-/-}$ mice (mean colony number and s.d. per 5,000 bone marrow cells). CFU, colony-forming units. **e**, Kaplan–Meier survival curves of *c-Cbl*$^{+/+}$, *c-Cbl*$^{+/-}$ and *c-Cbl*$^{-/-}$ mice carrying a *BCR-ABL* transgene, showing acceleration of blastic crisis in *c-Cbl*$^{+/-}$ and *c-Cbl*$^{-/-}$ mice. **f**, Wright–Giemsa staining of an enlarged lymph node in a *Bcr-Abl*$^{+}$ *c-Cbl*$^{-/-}$ mouse during blastic crisis shows massive infiltrates of immature leukaemic blasts. Original magnification, ×600.

Mouse LSK HSPCs expressed two Cbl family member proteins: wild-type c-Cbl and Cbl-b (Supplementary Fig. 12)[22]. When transduced into NIH3T3 cells stably expressing human epidermal growth factor receptor (EGFR), both Cbl proteins enhanced ubiquitination of EGFR after EGF stimulation, which was suppressed by coexpression of the C-CBL mutants (Fig. 3a, b). In haematopoietic cells, overexpression of wild-type C-CBL enhanced ligand-induced ubiquitination of a variety of tyrosine kinases, including c-KIT, FLT3 and JAK2. In contrast, C-CBL mutants not only showed compromised enzymatic activity, but also inhibited the ubiquitinating activities in these haematopoietic cells (Fig. 3c), leading to prolonged tyrosine kinase activation after ligand stimulation (Fig. 3d).

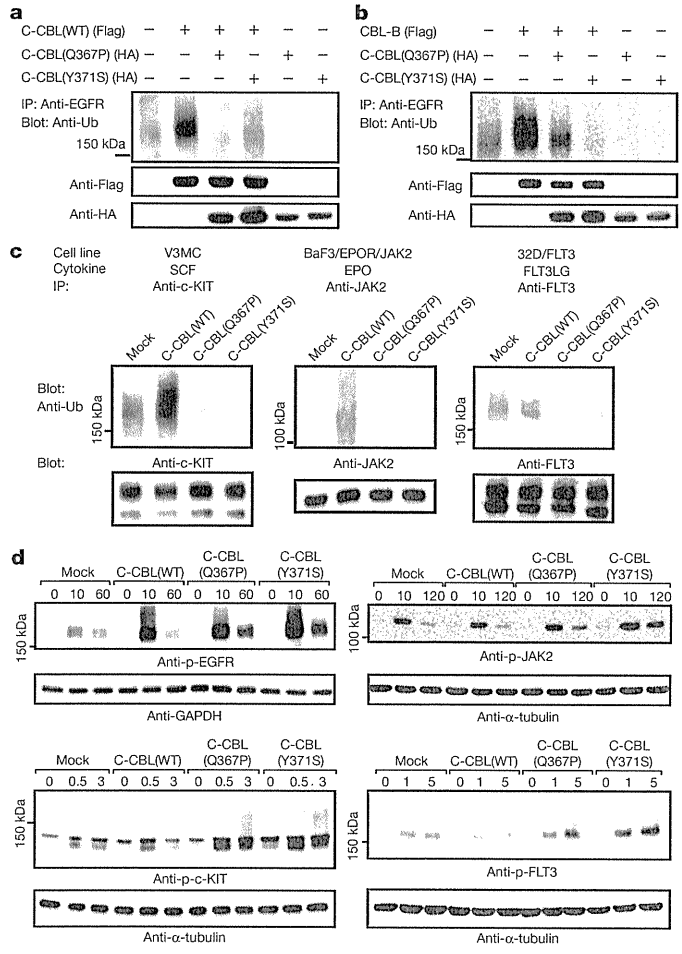

Figure 3 | Inhibitory actions of C-CBL mutants on wild-type C-CBL. **a**, **b**, Flag-tagged wild-type C-CBL (**a**) or CBL-B (**b**) were transfected into NIH3T3 cells stably transduced with human EGFR plus indicated HA-tagged C-CBL mutants. Anti-ubiquitin blots of immunoprecipitated EGFR after EGF stimulation show the inhibitory actions of the C-CBL mutants on ubiquitinating activity of C-CBL (**a**) and CBL-B (**b**). Bottom panels are anti-HA and anti-Flag blots of total cell lysates. **c**, Effects of wild-type and mutant C-CBL on cytokine-induced ubiquitination of c-KIT, JAK2 and FLT3 in haematopoietic cells V3MC, BaF3 co-transduced with human erythropoietin receptor (EPOR) and JAK2 (BaF3/EPOR/JAK2), and FLT3-transduced 32D (32D/FLT3), respectively. Each cell line was further transduced with indicated C-CBL mutants, and ubiquitination of immunoprecipitated kinases was detected by anti-ubiquitin blots at 1 min after stimulation with SCF, EPO and FLT3LG. Anti-kinase blots of the precipitated kinases are shown below each panel. **d**, Kinase phosphorylation was examined at indicated time points (shown in minutes) after ligand stimulation using immunoblot analyses of total cell lysates using antibodies to phosphorylated (p-) EGFR, c-KIT, JAK2 and FLT3 in which anti-α-tubulin or anti-GAPDH blots are provided as a control.

Because tyrosine kinase signalling is central to cytokine responses in haematopoietic cells and its deregulation is a common feature of myeloproliferative disorders[23], we next examined the effects of *C-CBL* mutations (*C-CBL*(Gln367Pro) and *C-CBL*(Tyr371Ser)) and the loss of wild-type *C-CBL* alleles on the responses of LSK HSPCs to various cytokines. In serum-free conditions, *c-Cbl*$^{-/-}$ LSK cells showed a modestly enhanced proliferative response to a variety of cytokines, including SCF, IL3 and TPO, compared to *c-Cbl*$^{+/+}$ cells (mock columns in Fig. 4a). However, the enhanced response in *c-Cbl*$^{-/-}$ cells was markedly augmented and extended to a broader spectrum of cytokines, including FLT3 ligand by the transduction of *C-CBL* mutants. Of note, the effect of *C-CBL* mutant transduction was not remarkable in *c-Cbl*$^{+/+}$ LSK cells except for the response to SCF, which was clearly enhanced by *C-CBL* mutants

©2009 Macmillan Publishers Limited. All rights reserved

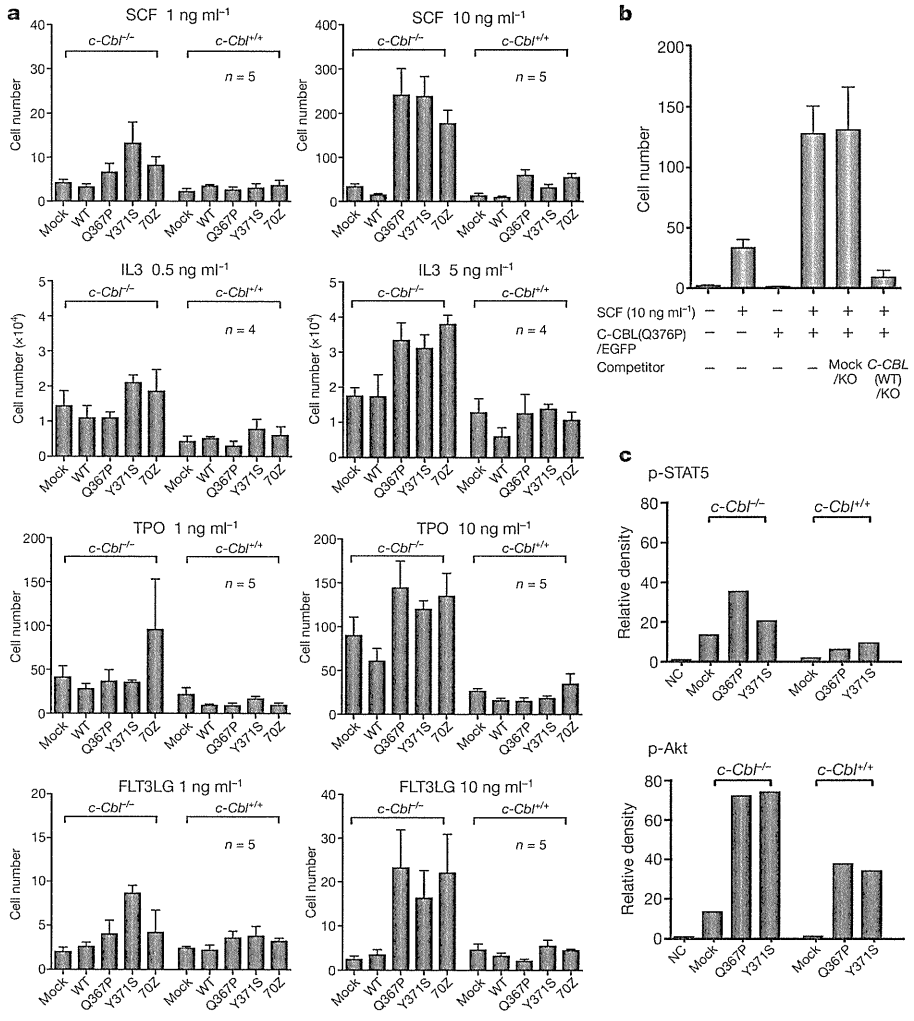

Figure 4 | Gain-of-function of mutant C-CBL augmented by loss of wild-type C-CBL. **a**, *c-Cbl*$^{+/+}$ and *c-Cbl*$^{-/-}$ LSK cells were transfected with various *C-CBL* internal ribosome entry site (IRES)/green fluorescent protein (GFP) constructs, and 50 GFP-positive cells were sorted for serum-free culture containing indicated concentrations of SCF, IL3, TPO and FLT3LG. Mean cell numbers (plus s.e.m.) on day 5 are plotted. **b**, *c-Cbl*$^{-/-}$ LSK cells were co-transduced with C-CBL(Gln367Pro)-IRES-EGFP (C-CBL(Q367P)/EGFP) and mock-IRES-Kusabira-Orange (mock/KO) or wild-type *C-CBL*-IRES-Kusabira-Orange (*C-CBL*(WT)/KO), and 50 GFP/KO double-positive cells were sorted into each well for cell proliferation assays in serum-free culture containing 10 ng ml^{-1} SCF. Mean cell numbers on day 5 (plus s.e.m., $n = 5$) are plotted. **c**, Ten thousand *c-Cbl*$^{+/+}$ and *c-Cbl*$^{-/-}$ LSK cells transduced with various C-CBL constructs were stimulated with 10 ng ml^{-1} SCF and 10 ng ml^{-1} TPO for 15 min. Total cell lysates were analysed by immunoblotting, using antibodies to STAT5, Akt and their phosphorylated forms. The intensities of phosphorylated proteins relative to total STAT5 (top panel) and Akt (bottom panel) are plotted. NC indicates the mean background signal obtained with nonspecific IgG.

even with a *c-Cbl*$^{+/+}$ background (Fig. 4a and Supplementary Fig. 13). To clarify further the effect of wild-type C-CBL on C-CBL mutants, both wild-type C-CBL and C-CBL mutants were co-transduced into *c-Cbl*$^{-/-}$ LSK cells, and their effects on the response to SCF were examined. As shown in Fig. 4b, the hyperproliferative response induced by C-CBL mutants was almost completely abolished by the co-transduction of wild-type C-CBL, suggesting the pathogenic importance of loss of wild-type *C-CBL* alleles found in most *C-CBL*-mutated cases. LSK cells transduced with C-CBL mutants also showed enhanced activation of the STAT5 and Akt pathways on cytokine stimulation (SCF and TPO), which was more pronounced in *c-Cbl*$^{-/-}$ than *c-Cbl*$^{+/+}$ LSK cells (Fig. 4c and Supplementary Fig. 14).

The modest enhancement of sensitivity to cytokines found in *c-Cbl*$^{-/-}$ LSK cells was a consequence of loss of C-CBL functions. In contrast, the hypersensitive response of mutant-transduced *c-Cbl*$^{-/-}$ LSK cells to a broad spectrum of cytokines represents gain-of-function of the mutants that could not be ascribed to a simple loss of C-CBL functions, which was also predicted from the strong association of *C-CBL* mutations with 11q-aUPD by analogy to the gain-of-function *JAK2* mutations associated with 9p-aUPD in polycythemia vera[2]. The gain-of-function of C-CBL mutants became more evident under a *c-Cbl*$^{-/-}$ background. The hypersensitive response to cytokines induced by mutant C-CBL under the *c-Cbl*$^{-/-}$ background was largely offset by the presence of the wild-type *c-Cbl* allele or by the transduction of the wild-type C-CBL gene, suggesting that the gain-of-function could be closely related to loss of C-CBL-like functions, probably by inhibition of Cbl-b. Supporting this view is a previous report that *c-Cbl/Cbl-b* double knockout T cells showed more profound impairments in the downregulation of the T-cell receptor (TCR), more sustained TCR signalling, and more vigorous proliferation, than *c-Cbl* or *Cbl-b* single knockout T cells after anti-CD3 (also known as CD3e) stimulation[24]. This is analogous to the gain-of-function found in some TP53 mutants, which has been explained by functional inhibition of two TP53 homologues, TP73 and TP63 (refs 25, 26). Of note, TP53 was also originally isolated as an oncogene through its mutated forms[27]. The Cbl-b inhibition-based gain-of-function model could be tested directly by comparing the behaviour of *c-Cbl/Cbl-b* double knockout LSK cells with that of LSK cells carrying homozygously knocked-in mutant *C-CBL* alleles. On the other hand, there remains a possibility that the gain-of-function could be mediated by a mechanism other than the simple inhibition of the homologue, because C-CBL mutants retained several motifs

©2009 Macmillan Publishers Limited. All rights reserved

that interacted with numerous signal-transducing molecules. Furthermore, considering the ubiquitous expression of CBL proteins, it would be of interest to explore the possible involvement of mutations in all *CBL* family members in other human cancers.

METHODS SUMMARY

Genomic DNA from 222 bone marrow samples with myeloid neoplasms were analysed using GeneChip SNP-genotyping microarrays (Affymetrix GeneChip) as described[28]. Allelic imbalances were detected from the allele-specific copy numbers calculated using CNAG/AsCNAR software (http://www.genome.umin.jp)[9,10]. *C-CBL* mutations were examined by sequencing PCR-amplified genomic DNA. For functional assays, haemagglutinin (HA)- or Flag-tagged complementary DNAs of wild-type and mutant *C-CBL* were generated by *in vitro* mutagenesis, constructed into a MSCV-based retroviral vector, pGCDNsamIRESGFP or pGCDNsamIRESKO, and used for retrovirus-mediated gene transfer. For the evaluation of oncogenicity of C-CBL mutants, NIH3T3 cells were transfected with various *C-CBL* constructs and used for colony assays in soft agar and tumour formation assays in nude mice. *c-Cbl*-deficient mice were generated using a conventional strategy of gene-targeting and crossed with *BCR-ABL* transgenic mice to evaluate the effect of the $c\text{-}Cbl^{-}$ allele on the acceleration of blastic crisis. LSK cells sorted from $c\text{-}Cbl^{+/+}$ and $c\text{-}Cbl^{-/-}$ mice were transduced with various *C-CBL* constructs. Their responses to cytokines were evaluated by cell proliferation assays, followed by immunoblot analyses of c-KIT, FLT3 and JAK2, as well as their downstream signalling molecules. The effects of C-CBL mutant expression on the ubiquitination of EGFR, c-KIT, FLT3 and JAK2 were examined by transducing C-CBL mutants into relevant cells, followed by anti-ubiquitin blots of the immunoprecipitated kinases after ligand stimulation. Functional competition of C-CBL mutants with wild-type C-CBL was assessed by cell proliferation assays of LSK cells co-transduced with both wild-type and mutant C-CBL genes. This study was approved by the ethics boards of the University of Tokyo, Chang Gung Memorial Hospital and Showa University. Antibodies and primers used in this study are listed in Supplementary Tables 8 and 9.

Full Methods and any associated references are available in the online version of the paper at www.nature.com/nature.

Received 9 October 2008; accepted 30 June 2009.
Published online 20 July 2009.

1. Knudson, A. G. Two genetic hits (more or less) to cancer. *Nature Rev. Cancer* 1, 157–162 (2001).
2. James, C. *et al.* A unique clonal JAK2 mutation leading to constitutive signalling causes polycythaemia vera. *Nature* 434, 1144–1148 (2005).
3. Ryan, P. E. *et al.* Regulating the regulator: negative regulation of Cbl ubiquitin ligases. *Trends Biochem. Sci.* 31, 79–88 (2006).
4. Schmidt, M. H. & Dikic, I. The Cbl interactome and its functions. *Nature Rev. Mol. Cell Biol.* 6, 907–918 (2005).
5. Thien, C. B. & Langdon, W. Y. Cbl: many adaptations to regulate protein tyrosine kinases. *Nature Rev. Mol. Cell Biol.* 2, 294–307 (2001).
6. Thien, C. B. & Langdon, W. Y. c-Cbl and Cbl-b ubiquitin ligases: substrate diversity and the negative regulation of signalling responses. *Biochem. J.* 391, 153–166 (2005).
7. Corey, S. J. *et al.* Myelodysplastic syndromes: the complexity of stem-cell diseases. *Nature Rev. Cancer* 7, 118–129 (2007).
8. Jaffe, E., Harris, N., Stein, H. & Vardiman J. *World Health Organization Classification of Tumours: Pathology and Genetics of Tumours of Haematopoietic and Lymphoid Tissues* 62–73 (IARC Press, 2002).
9. Nannya, Y. *et al.* A robust algorithm for copy number detection using high-density oligonucleotide single nucleotide polymorphism genotyping arrays. *Cancer Res.* 65, 6071–6079 (2005).
10. Yamamoto, G. *et al.* Highly sensitive method for genomewide detection of allelic composition in nonpaired, primary tumor specimens by use of affymetrix single-nucleotide-polymorphism genotyping microarrays. *Am. J. Hum. Genet.* 81, 114–126 (2007).
11. Haase, D. Cytogenetic features in myelodysplastic syndromes. *Ann. Hematol.* 87, 515–526 (2008).
12. Langdon, W. Y. *et al.* v-cbl, an oncogene from a dual-recombinant murine retrovirus that induces early B-lineage lymphomas. *Proc. Natl Acad. Sci. USA* 86, 1168–1172 (1989).
13. Abbas, S. *et al.* Exon 8 splice site mutations in the gene encoding the E3-ligase CBL are associated with core binding factor acute myeloid leukemias. *Haematologica* 93, 1595–1597 (2008).
14. Caligiuri, M. A. *et al.* Novel c-CBL and CBL-b ubiquitin ligase mutations in human acute myeloid leukemia. *Blood* 110, 1022–1024 (2007).
15. Sargin, B. *et al.* Flt3-dependent transformation by inactivating c-Cbl mutations in AML. *Blood* 110, 1004–1012 (2007).
16. Dunbar, A. J. *et al.* 250K single nucleotide polymorphism array karyotyping identifies acquired uniparental disomy and homozygous mutations, including novel missense substitutions of c-Cbl, in myeloid malignancies. *Cancer Res.* 68, 10349–10357 (2008).
17. Zheng, N. *et al.* Structure of a c-Cbl-UbcH7 complex: RING domain function in ubiquitin-protein ligases. *Cell* 102, 533–539 (2000).
18. Murphy, M. A. *et al.* Tissue hyperplasia and enhanced T-cell signalling via ZAP-70 in c-Cbl-deficient mice. *Mol. Cell. Biol.* 18, 4872–4882 (1998).
19. Naramura, M. *et al.* Altered thymic positive selection and intracellular signals in Cbl-deficient mice. *Proc. Natl Acad. Sci. USA* 95, 15547–15552 (1998).
20. Rathinam, C. *et al.* The E3 ubiquitin ligase c-Cbl restricts development and functions of hematopoietic stem cells. *Genes Dev.* 22, 992–997 (2008).
21. Honda, H. *et al.* Acquired loss of p53 induces blastic transformation in p210(bcr/abl)-expressing hematopoietic cells: a transgenic study for blast crisis of human CML. *Blood* 95, 1144–1150 (2000).
22. Zeng, S. *et al.* Regulation of stem cell factor receptor signaling by Cbl family proteins (Cbl-b/c-Cbl). *Blood* 105, 226–232 (2005).
23. Kaushansky, K. Hematopoietic growth factors, signaling and the chronic myeloproliferative disorders. *Cytokine Growth Factor Rev.* 17, 423–430 (2006).
24. Naramura, M. *et al.* c-Cbl and Cbl-b regulate T cell responsiveness by promoting ligand-induced TCR down-modulation. *Nature Immunol.* 3, 1192–1199 (2002).
25. Dittmer, D. *et al.* Gain of function mutations in p53. *Nature Genet.* 4, 42–46 (1993).
26. Lang, G. A. *et al.* Gain of function of a p53 hot spot mutation in a mouse model of Li-Fraumeni syndrome. *Cell* 119, 861–872 (2004).
27. Finlay, C. A., Hinds, P. W. & Levine, A. J. The p53 proto-oncogene can act as a suppressor of transformation. *Cell* 57, 1083–1093 (1989).
28. Chen, Y. *et al.* Oncogenic mutations of ALK kinase in neuroblastoma. *Nature* 455, 971–974 (2008).

Supplementary Information is linked to the online version of the paper at www.nature.com/nature.

Acknowledgements This work was supported by the Core Research for Evolutional Science and Technology, Japan Science and Technology Agency, a Grant-in-Aid from the Ministry of Health, Labor and Welfare of Japan and from the Ministry of Education, Culture, Sports, Science and Technology, and a grant from National Health Research Institute, Taiwan, NHRI-EX96-9434SI, and NIH-2R01CA026038-30. We thank W. Y. Langdon for providing a human *C-CBL* cDNA. A mast-cell cell line expressing c-KIT V3MC was a gift from M. F. Gurish. We also thank Y. Ogino and K. Fujita for their technical assistance.

Author Contributions M.S. and M.Kato performed microarray experiments and subsequent data analyses. T.S., T.Y., H.Honda and H.Hirai generated and analysed *c-Cbl*-null mice. M.S., M.Otsu, S.Y., M.N., K.K., N.G., M.Onodera, M.S.-Y. and H.N. conducted functional assays of C-CBL mutants. L.-Y.S., M.S., M.Kato, K.N., J.T. and A.T. performed mutation analysis. H.O. performed pathological analysis of *c-Cbl*-null mice. L.-Y.S., N.K., H.Harada, M.Kurokawa, S.C., H.M., H.P.K. and M.Omine prepared MDS specimens. M.S., M.Otsu, Y.H., K.O., H.M., H.N., L.-Y.S., H.P.K. and S.O. designed the overall study, and S.O. wrote the manuscript. All authors discussed the results and commented on the manuscript.

Author Information Full copy number data for the 222 samples are accessible from the Gene Expression Omnibus public database (http://ncbi.nlm.nih.gov/geo/) with the accession number GSE15187. Reprints and permissions information is available at www.nature.com/reprints. Correspondence and requests for materials should be addressed to S.O. (sogawa-tky@umin.ac.jp) or L.-Y.S. (sly7012@adm.cgmh.org.tw).

©2009 Macmillan Publishers Limited. All rights reserved

METHODS

Genome-wide analysis of allelic imbalances in primary myeloid neoplasms. Bone marrow specimens were obtained from 222 patients diagnosed with myeloid neoplasms according to the WHO classification (Supplementary Tables 1 and 2). High molecular weight genomic DNA was extracted and used for microarray analysis using Affymetrix GeneChip 50K XbaI, HindIII or 250K NspI, according to the manufacturer's instructions. Genome-wide detection of allelic imbalances was performed using CNAG/AsCNAR software (http://www.genome.umin.jp)[9,10].

Mutation analysis. Mutation analysis was performed by direct sequencing of PCR-amplified coding exons of the relevant genes, using an ABI PRISM 3100 genetic analyser (Applied Biosystems). The target genes, exons and PCR primers are listed in Supplementary Table 8. Tandem duplication of the *FLT3* gene was examined by genomic PCR and sequencing.

Preparation of high-titre vesicular stomatitis virus glycoprotein (VSV-G)-pseudotyped retroviral particles. HA-tagged human *C-CBL* cDNA was a gift from W. Y. Langdon. Nine mutant cDNAs of *C-CBL*, including eight from patients' specimens and a 70Z mutant corresponding to a mutant isolated from mouse lymphoma[29], were generated on the basis of this construct, using a QuickChange site-directed mutagenesis kit (Stratagene). These were then constructed into the retrovirus vectors pGCDNsamIRESGFP and pGCDNsamIRESKO[30–32]. Vector plasmids were co-transfected with a VSV-G cDNA into 293GP cells (provided by R. C. Mulligan) to obtain retrovirus-containing supernatant, which was then transduced into 293GPG cells to establish stable cell lines capable of producing VSV-G-pseudotyped retroviral particles on induction[33,34]. The average titre of retrovirus stocks prepared from these cell lines routinely exceeded approximately $1–10 \times 10^7$ inclusion-forming units per ml, as estimated using Jurkat cells.

Assays for anchorage-independent growth and tumorigenicity in nude mice. NIH3T3 cells (the Japan Cell Resource Bank) were stably transduced with wild-type and mutant *C-CBL* by retrovirus-mediated gene transfer. For colony formation assays, 1.0×10^3 stable cells for each construct were inoculated in 0.33% top agar, and the numbers of colonies >1 mm in diameter were counted 3 weeks after inoculation ($n = 8$). Experiments were repeated four times. For tumour formation in nude mice, 1.0×10^7 stable cells were inoculated subcutaneously at two sites per mouse. Cells were inoculated at six sites in three mice for each construct.

Purification of LSK HSPCs. LSK HSPCs were purified from bone marrow and spleen as described[35,36]. Multicolour flow cytometry analysis and cell sorting were performed using a MoFlo cell Sorter (Beckman Coulter). The purity of sorted cell fractions consistently exceeded 98%.

Replating assays of bone marrow progenitor cells. Bone marrow LSK cells were infected with IRES/GFP-containing retrovirus carrying mock, wild-type C-CBL and three C-CBL mutants (C-CBL(Gln367Pro), C-CBL(Tyr371Ser) and C-CBL(Cys384Gly)) as well as C-CBL(70Z) on RetroNectin-coated dishes. After 48 h infection in culture in StemSpan supplemented with SCF (50 ng ml^{-1}; Peprotech), TPO (20 ng ml^{-1}) and FLT3LG (20 ng ml^{-1}), 1.0×10^2 GFP-positive cells were inoculated in MethoCult M3231 supplemented with TPO (20 ng ml^{-1}), IL3 (10 ng ml^{-1}), IL6 (10 ng ml^{-1}), FLT3LG (10 ng ml^{-1}) and SCF (50 ng ml^{-1}) for colony formation. Colony-forming cells were collected 7 days after each inoculation, from which 1.0×10^3 cells were repeatedly subjected to replating until no colonies were produced. Experiments were repeated at the indicated times for each C-CBL construct.

Generation of *c-Cbl*$^{-/-}$ mice and evaluation of their tumour-prone phenotype. *c-Cbl*$^{-/-}$ mice were generated using a conventional method of gene targeting (Supplementary Fig. 10). *c-Cbl*$^{+/+}$, *c-Cbl*$^{+/-}$ and *c-Cbl*$^{-/-}$ mice were crossed with *BCR-ABL* transgenic mice, and their survival and the development of blastic crises were monitored.

Evaluation of haematopoietic pool size in *c-Cbl*$^{-/-}$ mice. LSK and CD34$^-$ LSK cells were sorted from bone marrow cells or spleens of *c-Cbl*$^{-/-}$ mice, and their numbers were compared to those in *c-Cbl*$^{+/+}$ littermates (8 week old). Approximately 5×10^3 bone marrow cells collected from *c-Cbl*$^{+/+}$ and *c-Cbl*$^{-/-}$ mice were inoculated into MethoCult M3231 culture supplemented with TPO (20 ng ml^{-1}), IL3 (10 ng ml^{-1}), IL6 (10 ng ml^{-1}), EPO (3 U ml^{-1}) and SCF (50 ng ml^{-1}). The number of colonies was counted 7 days after culturing.

***In vitro* cell proliferation assays.** Approximately 6×10^3 LSK cells from *c-Cbl*$^{-/-}$ mice and their *c-Cbl*$^{+/+}$ littermates (8 week old) were sorted into RetroNectin-coated 96-well U-bottom plates containing α-minimum essential medium supplemented with 1% fetal bovine serum (FBS), mouse SCF (50 ng ml^{-1}), and human TPO (100 ng ml^{-1}). After 24 h pre-incubation, retrovirus supernatant was added to each well at a multiplicity of infection of about 10. The plates were incubated for another 24 h in the presence of protamine sulphate (10 μg ml^{-1}), followed by repeated infection and extended culture for 2 days in S-Clone SF-O3 medium (Sanko Junyaku) supplemented with 1% BSA, 50 ng ml^{-1} SCF and 50 ng ml^{-1} TPO. On day 4, fluorescent-marker-positive cells were sorted for subsequent analyses. Cell survival and proliferation of LSK cells transduced with different *C-CBL* constructs were assessed in serum-free liquid culture in 96-well U-bottom plates in the presence of various cytokines. Each well received 50 fluorescent-marker-positive LSK cells, and the cells were cultured in S-Clone supplemented with 1% BSA plus SCF, TPO, IL3 or FLT3LG at the indicated concentrations. Cell numbers were counted either by analysing well images or by flow cytometry using FlowCount beads (Beckman Coulter). After 6 h serum starvation, 1×10^4 LSK cells transduced with various *C-CBL* constructs were stimulated with SCF (10 ng ml^{-1}) and TPO (10 ng ml^{-1}) for 15 min. Whole-cell lysates were examined for activation of STAT5 and Akt by immunoblots using the respective antibodies.

Immunoblot analysis of physical interactions between mutant C-CBL and CBL-B. Flag-tagged CBL-B or C-CBL was co-transfected into NIH3T3 cells with each of three HA-tagged C-CBL mutants (C-CBL(Gln367Pro), C-CBL(Tyr371Ser) and C-CBL(70Z)). Total cell lysates of these NIH3T3 cells were immunoprecipitated with anti-Flag antibody, followed by immunoblot analysis with anti-HA antibody.

Detection of ubiquitination and phosphorylation of kinases. After overnight serum starvation, NIH3T3 cells stably transduced with human EGFR, and indicated HA-tagged C-CBL mutants and Flag-tagged wild-type C-CBL were stimulated with human EGF (10 ng ml^{-1}) for 2 min. Cell lysates were immunoprecipitated with anti-EGF antibody, followed by immunoblotting using anti-ubiquitin antibody. Constructs for wild-type C-CBL and mutant C-CBL were stably transduced into a mast cell line, V3MC, FLT3-transduced 32D cells (32D/FLT3) and BaF3 cells transduced with human EPOR and JAK2 (BaF3/EPOR/JAK2) using retrovirus-mediated gene transfer. After overnight serum starvation, the transduced cells were stimulated with 10 ng ml^{-1} SCF (V3MC), 10 U ml^{-1} EPO (BaF3/EPOR/JAK2) or 10 ng ml^{-1} FLT3LG (32D/FLT3) for 1 min. The specific kinases were immunoprecipitated with relevant antibodies, and their ubiquitination was detected by immunoblotting with anti-ubiquitin antibody. Tyrosine phosphorylation of EGFR, c-KIT, JAK2 and FLT3 was examined by immunoblot analyses of total cell lysates after cytokine stimulation at indicated time points, using antibodies specifically recognizing phosphorylated kinases, anti-p-EGFR, anti-p-c-KIT, anti-p-JAK2 and anti-p-FLT3, respectively. Anti-GAPDH or anti-α-tubulin immunoblot was performed as a control. Antibodies used in this study are listed in Supplementary Table 9.

Statistical analysis. Statistical significance of prolonged replating capacity of mutant *C-CBL*-transduced LSK cells was tested by counting the total number of dishes that produced colonies, followed by Fisher's exact test. Survival curves of *c-Cbl*$^{+/+}$, *c-Cbl*$^{+/-}$ and *c-Cbl*$^{-/-}$ mice containing the *BCR-ABL* transgene were generated using the Kaplan–Meier method. Overall survivals of *C-CBL*-mutated and non-mutated CMML cases were analysed according to the proportional hazard model, using STATA software. Statistical differences in survival were evaluated using the log-rank test, and statistical differences in 2×2 contingency tables were tested according to Fisher's exact method. Student's *t*-tests were used to evaluate the significance of difference in spleen mass, number of haematopoietic progenitors and colony-forming cells between *c-Cbl*$^{+/+}$ and *c-Cbl*$^{-/-}$.

29. Blake, T. J. *et al.* The sequences of the human and mouse c-cbl proto-oncogenes show v-cbl was generated by a large truncation encompassing a proline-rich domain and a leucine zipper-like motif. *Oncogene* 6, 653–657 (1991).
30. Hamanaka, S. *et al.* Stable transgene expression in mice generated from retrovirally transduced embryonic stem cells. *Mol. Ther.* 15, 560–565 (2007).
31. Nabekura, T. *et al.* Potent vaccine therapy with dendritic cells genetically modified by the gene-silencing-resistant retroviral vector GCDNsap. *Mol. Ther.* 13, 301–309 (2006).
32. Sanuki, S. *et al.* A new red fluorescent protein that allows efficient marking of murine hematopoietic stem cells. *J. Gene Med.* 10, 965–971 (2008).
33. Ory, D. S., Neugeboren, B. A. & Mulligan, R. C. A stable human-derived packaging cell line for production of high titer retrovirus/vesicular stomatitis virus G pseudotypes. *Proc. Natl Acad. Sci. USA* 93, 11400–11406 (1996).
34. Suzuki, A. *et al.* Feasibility of *ex vivo* gene therapy for neurological disorders using the new retroviral vector GCDNsap packaged in the vesicular stomatitis virus G protein. *J. Neurochem.* 82, 953–960 (2002).
35. Ema, H. *et al.* Adult mouse hematopoietic stem cells: purification and single-cell assays *Nature Protoc.* 1, 2979–2987 (2006).
36. Osawa, M. *et al.* Long-term lymphohematopoietic reconstitution by a single CD34-low/negative hematopoietic stem cell. *Science* 273, 242–245 (1996).

©2009 Macmillan Publishers Limited. All rights reserved

European Journal of Haematology ISSN 0902-4441

ORIGINAL ARTICLE

Aberrant p53 protein expression and function in a panel of hematopoietic cell lines with different p53 mutations

Shimeru Kamihira[1], Chiharu Terada[1], Daisuke Sasaki[1], Katsunori Yanagihara[1], Kunihiro Tsukasaki[2], Hiroo Hasegawa[1], Yasuaki Yamada[1]

Departments of [1]Laboratory Medicine and [2]Hematology, Nagasaki University Graduate School of Biomedical Sciences, Nagasaki, Japan

Abstract

The *p53* gene is one of the most important genes involved in carcinogenesis and its role in part has been clarified by research using cell lines. To know the comprehensive characteristics of 22 hematopoietic cell lines (T, 13 and non-T, nine lines), the relationship between p53 mutational status, its altered functioning, and its mRNA and protein levels were examined. p53 mutations were less frequent in T-cell lines (38% vs. 78%) with mainly single nucleotide substitutions generating missense codons. Of 22 different p53 mutations, 12 (54.5%) resulted in mutated proteins, with the mutations clustering mainly in the sequence-specific DNA-binding site region located from amino acid residues 102 to 292. *p53* mRNA and protein assays determined that wild-type cell lines expressed constant levels of both mRNA and protein, but mutated cell lines demonstrated two expression patterns: protein over-expression with reduced mRNA levels, because of missense mutations; and protein under-expression with little mRNA expression, because of other mutations. The resistance to Nutlin (MDM2 inhibitor)-induced apoptosis was associated with p53 mutations independently of MDM2 expression levels. This clarification of the unique associations in cell lines useful for bio-medical studies will contribute to a better understanding of p53-associated carcinogenesis.

Key words p53; mutation; haplo-insufficiency; hematologic cell line; adult T-cell leukemia

Correspondence Shimeru Kamihira, PhD, MD, Department of Laboratory Medicine, Nagasaki University Graduate School of Biomedical Sciences, 1-7-1, Sakamoto, Nagasaki 852-8501, Japan. Tel: +81 95 819 7407; Fax: +81 95 819 7422; e-mail: kamihira@nagasaki-u.ac.jp

Accepted for publication 22 December 2008

doi:10.1111/j.1600-0609.2009.01211.x

The tumor suppressor gene *p53* is located on the short arm of chromosome 17 and plays a central role in control of the cell cycle, DNA repair, and activation of apoptosis. Abrogation of these *p53* functions is thought to be involved in carcinogenesis (1, 2). *p53* knockout mice have an increased tendency to develop spontaneous tumors. It was previously thought that transformation required the inactivation of both *p53* alleles, i.e., loss of heterozygosity, but recent studies have shown that *p53* function can also be disrupted by haplo-insufficiency; i.e., the alteration of one allele of the gene with the other allele remaining normal (3). Inactivation of the *p53* gene is known to be caused by genetic and epigenetic mechanisms, such as mutation, methylation, and interaction with viral proteins. *p53* alterations are widely observed in at least 50% of human tumors, including hematologic malignancies, with colon, breast, and lung cancers having the highest frequencies of *p53* mutations (2, 4).

Mutant p53 proteins encoded by mutated alleles have several characteristics that differ from those of wild-type p53, including a longer half-life and a dominant negative effect on wild-type p53. Furthermore, the dominant negative function seems to vary according to the polymorphic status of codon 72 (C466G; arginine vs. proline) (5). These characteristics of the mutant protein appear to account for its over-expression in tumor cells harboring the mutated gene, and which demonstrate biologically aggressive behavior and chemoresistance (6–8). The presence of *p53* mutations and over-expression of p53 protein has a strong prognostic impact (9, 10). Several studies

© 2009 The Authors
Journal compilation **82** (301–307) © 2009 Blackwell Munksgaard

have reported that adult T-cell leukemia (ATL) patients demonstrate mutational inactivation of p53 in 20–40% of cases, and that gene inactivation contributes to the development of malignant phenotypes (11).

The Nutlins, *cis*-imidazoline analogs, are novel small-molecule inhibitors of MDM2, which bind to MDM2, releasing them from negative control by the p53 pathway and leading to effective p53 stabilization and activation in wild-type cells (12). However, little is known about the association between *p53* mutational status and expression levels and functioning of p53 protein. Accordingly, using a panel of hematopoietic cell lines available as bio-source to study oncology, we examined the associations between *p53* mutations, p53 functional status, and mRNA and protein levels.

Materials and methods

Cell lines

The hematopoietic cell lines used included six ATL-derived T-cell lines, three human T-cell leukemia virus type-1 (HTLV-1)-infected T-cell lines, four T-cell lines without HTLV-1, five lymphoma-derived B-cell lines, two monocytic cell lines, and two others. All but three (MT1, MT2, and HUT102) of the ATL cell lines were established in our laboratory (13). The other cell lines were obtained from the American Type Culture Collection (Rockville, MD, USA), and the Hayashibara Bio Inc (Okayama, Japan). Each cell line was cultured according to the supplier's, or our, protocols.

High molecular weight DNA was extracted from cell lines using a QIAmp DNA Blood Mini kit (Qiagen GmbH, Hilden, Germany). Total RNA was extracted using ISOGEN (Nippon Gene, Toyama, Japan). After removing contaminating genomic DNA using a Message Clean kit, cDNA was synthesized using Oligo (dT) 12–18 Primer and SuperScript III Reverse Transcriptase (Invitrogen Corp., Carlsbad, CA, USA). All primers and probes used in this study were designed using Primer3Plus (14) (The sequences of all primers and probes used here are available via an e-mail of kamihira@nagasaki-u.ac.jp).

Mutational analysis

A 1376-bp fragment including the *p53* mRNA open reading frame (ORF) was amplified by polymerase chain reaction (PCR) using primers S1 and AS1. The standard thermal cycling conditions were an initial 98°C for 30 s followed by 35 cycles at 98°C for 10 s and 67°C for 1 min. The amplicons were subjected to direct sequencing analysis to identify mutations in the *p53* ORF. The PCR primers used for cycle sequencing were S1, S2, and S3 for anti-sense products, and AS1, AS2, and AS3 for sense products. Cycle sequencing was performed using a BigDye Terminator v3.1 Cycle Sequencing Kit (Applied Biosystems, Foster City, CA, USA) and an Automated DNA Sequence Analyzer (Model 3100; Applied Biosystems, Foster City, CA, USA). Sequence data for the *p53* ORF region were compared with the published *p53* mRNA sequence (NM_00546).

Real time RT-PCR quantification for *p53* and *mdm2* mRNA levels

Primers and TaqMan probes labeled with TAMRA dye at the 3′ end and FAM at the 5′ end were designed. The mRNA levels for *p53*, *mdm2*, and porphobilinogen deaminase (*PBGD*) were measured from a cDNA template using a LightCycler480 PCR System (Roche Diagnostics, Mannheim, Germany). Briefly, reactions were performed in a 20 μL volume with 5 μL 1/10 diluted cDNA, 0.5 μM PCR primers, 0.1 μM TaqMan probes, and 10 μL of 20 LightCycler 480 probes (Master Mix; Roche Diagnostics). The PCR program consisted of 95°C for 5 min followed by 50 cycles of 95°C for 10 s and 60°C for 30 s. After 50 cycles, the absolute amounts of *p53*, *mdm2*, and *PBGD* mRNA were interpolated from the standard curves generated by the dilution method using plasmids derived from a clone transfected with pTAC-1 Vector (BioDynamics Laboratory Inc., Tokyo, Japan) containing amplicons from the *p53*, *mdm2*, and *PBGD* genes, respectively. To normalize these results for variability in concentration and integrity of RNA and cDNA, the *PBGD* gene was used as an internal control in each sample.

Measurement of p53 protein

Total p53 protein in cell lysates (10 μg) was measured using the Luminex$^{100™}$ System (Hitachi Software Engineering Co., Tokyo, Japan), and the total p53 Antibody Bead Kit (LHO0151, Biosource International, Camarillo, CA, USA), according to the manufacturers' instructions. In brief, cells were washed three times with phosphate-buffered saline and pelleted cells were homogenized at 4°C in lysis buffer (0.1% sodium dodecyl sulfate, 1% Igepal CA-630, and 0.5% sodium deoxycholate) and a protease inhibitor cocktail (Sigma, St Louis, MO, USA). Sample solutions appropriately diluted with assay diluent were incubated with anti-p53 antibody-coupled beads for 2 h at room temperature on an orbital plate shaker, washed three times with wash solution, and the beads were further incubated with biotinylated detector antibody for 1 h. This was followed by incubation with streptavidin–R-phycoerythrin for 30 min at room temperature, and washing, after which the suspended beads were analyzed using the Luminex$^{100™}$ System. A

© 2009 The Authors

standard curve was created using serially diluted recombinant p53, and the p53 concentrations in samples were estimated.

Assays for p53 activation

The degree of DNA-binding capacity and the phosphorylation at serine 15 ($p53^{ser15}$) were analyzed as markers of p53 activation, using a TransAM™ p53 Transcription Factor Assay kit (Active Motif, Carlsbad, CA, USA) and an anti-phospho-$p53^{ser15}$/total p53 Multiplex Bead-based system (BioSource International) available for Luminex technology. The degree of activation was demonstrated by the fold induction of the DNA-binding capacity of p53 and the fold induction of phosphorylation of $p53^{ser15}$, relative to the measures before and after treatment with Nutlin-3.

Briefly, nuclear extracts from cells treated with 10 μM Nutlin-3 (Sigma Aldrich, St Louis, MO, USA) for 24 h were diluted in 10 μg of total protein with lysis buffer and applied to plates with immobilized oligonucleotides containing the p53 consensus binding site. After 1 h at room temperature, plates were washed and incubated with p53 antibody, followed by secondary antibody and developing solution. Color generated as a marker of the DNA-binding capacity was read at 450 nm. The procedure was performed according to instructions for the TransAM™ p53 and the Luminex$^{100™}$.

The phosphorylation of $p53^{ser15}$ was analyzed using anti-p53 and anti-phospho $p53^{ser15}$ according to the Luminex$^{100™}$ system protocol, as described above. The final outcome of p53 activation was determined by the degree of apoptosis induced by Nutlin-3 using the annexin V/propidium iodide double staining flow-cytometric method (15).

Statistical analysis

The chi-squared and Fisher's exact tests were used to examine categorical data, and the Mann–Whitney *U*-test

Table 1 Characteristics of cell lines tested and summary of *p53* mutations and deduced amino acid sequences

Cell line	Origin	RT-PCR products	Event				p53 status
			Exon	Codon	Sequence	aa	
SO4	ATL cell	1.4 kb (Arg)[2]	6	223	C919A	Missense (Pro → His)	Mt
ST1	ATL cell	1.4 kb (Pro)					Wt
KK1	ATL cell	1.4 kb (Pro)	3	31	G342A	Missense (Val → Ire)	Mt
			5	152	C706T	Missense (Pro → Arg)	
KOB	ATL cell	1.4 kb (Pro)					Wt
LM-Y1	ATL cell	1.4 kb (Arg)	4	36	G359A	Silent	Wt
MT1	ATL cell	1.4 kb (Arg)	5	176	G778A	Missense (Cyt → Tyr)	Mt
OMT	HTLV-1 infected T	1.4 kb (Pro)					Wt
MT2	HTLV-1 infected T	1.4 kb (Arg)					Wt
HUT102	HTLV-1 infected T	1.4 kb (Arg)					Wt
MT1s	Non-HTLV-1 T	1.4 kb (Arg)	5	149	C697T	Missense (Ser → Phe)	Mt
MT1g	Non-HTLV-1 T	1.4 kb (Arg)					Wt
MOLT4	Non-HTLV-1 T	1.4 kb (Arg)					Wt
Jurkat	Non-HTLV-1 T	1.4 kb (Arg)	5	125	G626A	Missense (Thr → Arg)	Mt
			6	196	C837T	Nonsense (Stop)	
		1.2 kb (del)	4	59–125	425–625	Deletion 199[1]	
			10	360	1329(G)	Deletion 1[1]	
SuDHL	B-cell lymphoma	1.4 kb (Arg)					Wt
Ramos	B-cell lymphoma	1.4 kb (Arg)	7	254	A/T1011/2G/A	Missense (Ile → Asp)	Mt
SKW6.4	B-cell lymphoma	1.4 kb (Arg)					
		1.2 kb (Pro)	4	59–125	426-624	Deletion 199[1]	Mt
HS-sultan	Myeloma	1.4 kb (Pro)					Wt
CA46	Burkitt lymphoma	1.4 kb (Pro)	7	248	G994A	Missense	Mt
THP1	Monocytic leukemia	1.4 kb (Arg)	5	174–182	770–795	Deletion 25[1]	Mt
U937	Monocytic leukemia	1.4 kb (Arg)	4	105	G564A	Missense (Gly → Ser)	Mt
			5	125	G626A	Silent	
			6	196	C837T	Nonsense (stop)	
		1.2 kb (del)	4	59–125	425–625	Deletion 199[1]	
HL60	Myeloid leukemia	No-detected				Deletion	Mt
K562	Erythroblastic leukemia	1.4 kb (Pro)	5	135	655(C)	Insertion[1]	Mt

[1]Frame shift (stop codon).
[2]p53 codon 72 polymorphic status, C466G.

© 2009 The Authors

and Kruskal–Wallis tests were used for non-parametric data. Differences in the strength of the association between two variables were evaluated by the Spearman's rank correlation coefficients. Differences were considered statistically significant when *P*-values were <0.05.

Results

Mutation profiles of cell lines

Using the present RT-PCR protocol, two main, distinct products of about 1.4 and 1.2 kb were generated in Jurkat, U937, THP1, K562, and SKW6.4 cells, while the remaining 16 cell lines, excluding HL-60 cells, showed a single band of 1.4 kb. No amplified products were observed in HL-60 cells. The results from direct sequencing of the amplicons are summarized in Table 1. Overall, 20 *p53* mutations were identified in 13 of 22 cell lines (59.0%). The mutations were located in exons 3 (one event), 4 (five events), 5 (seven events), 6 (two events), 7 (two events), and elsewhere (two events). Clustering was observed in exons 4 and 6, which is a highly conserved region including the sequence specific DNA-binding sites from amino acids 102 to 292. Of the 20 mutations, 13 (65%) were single nucleotide substitutions, whereas six (30%) were found to be deletions or insertions with frame-shifts generating stop codons. The 13 single nucleotide substitutions consisted of nine missense (69.2%), two nonsense, and two silent mutations. Missense mutations were mainly detected in T-cell lines, whereas deletions and nonsense mutations were mainly detected in B-cell and myeloid cell lines. Fifteen of the 22 mutations, such as C919C, C706T, G342A, G359A, G778A, G778A, C697T, G626A, C626A, C837T, AT1011GA, G994A, 174-182del, G564A, and 655(ins C), were accordant with the previous reports (IARC TP Mutation Database and The TP53 Web site). On the other hand, four kinds of the mutations detected in Jurkat, SKW6.4 and U937 have not yet reported. In particular, 199 base pair deletion (nt 425–625) in exon 4 was detected in only the 1.2 kb PCR products, suggesting that it is derived from a splicing form. Consequently, five of 13 T-cell lines and seven of nine non-T-cell lines (totally 12/22, 54.5%) were deduced to carry mutant p53 proteins. Regarding the relationship between mutations and the genotype of the p53 codon 72 polymorphism (arginine vs. proline), mutations were demonstrated to be in arginine-encoding alleles in nine cell lines, and in proline-encoding alleles in three cell lines, indicating that mutations occurred more frequently in the arginine-encoding alleles (69.2% vs. 23.10%, $P = 0.04$), as shown in Tables 1 and 2.

Association of *p53* mutational status with its mRNA and protein levels

The *p53* mRNA levels differed significantly between the wild-type and the mutated cell lines (0.62 vs. 0.37 $P = 0.048$). The p53 protein levels varied widely from 0 to 15 000 pg/mL, but the mean values were not significantly different between the wild-type and the mutated cell lines (4160 vs. 3860 pg/mL). The p53 protein levels in all cell lines failed to correlate with the p53 mRNA levels, although specific cell lines with protein levels of <1000 pg/mL showed tendencies toward inverse correlations between *p53* mRNA and protein levels ($r = -0.4636$, the Spearman *U*-test), as shown in Fig. 1. Furthermore, Fig. 1 shows the distinctive distribution of the cell lines which formed three clusters, designated as A, B, and C. Wild-type cell lines clustered in the center area (A), representing balanced expressions of p53

Table 2 Comparison of *p53* codon 72 (C466G) polymorphic status in wild-type and mutated groups

		p53 codon 72 (C466G) status		
p53 mutation	*n* (%)	Arg (%)	Pro (%)	*Unknown (%)*[1]
Wild-type	9 (41.0)	5 (55.5)	4 (45.5)	*0*
Mutated	13 (59.0)	9 (69.2)*	3 (23.1)**	*1 (7.7)*
Total	22 (100)	14	7	*1*

The allelic frequency was dominant for the arginine-encoding allele compared to the proline-encoding allele (* vs. **; $P = 0.0405$).
[1]Unknown due to complete deletion.

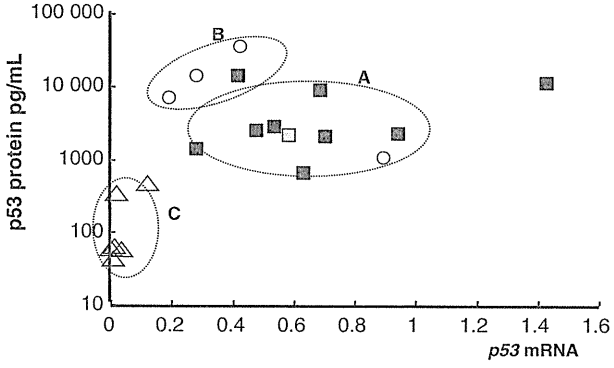

Figure 1 Twin dot graph of p53 protein (*Y*-axis) and mRNA (*X*-axis) expression levels in cell lines categorized according to their *p53* mutational status. Solid square; wild-type, open circle; missense, open triangle; other mutations, gray square; silent mutation. No correlation between *p53* mRNA and protein levels ($r = 0.238$, $P = 0.175$). However, a unique association among the types of mutations, *p53* mRNA and protein was observed, because solid squares are clustered into the central area (A), while mutated cells are separated into two clusters of B and C: The cell lines with wild-type sequences had balanced levels of transcripts and proteins, and cell lines with mutants were subdivided into two groups, with either over-expressed or under-expressed protein levels, with low mRNA expression.

© 2009 The Authors
Journal compilation **82** (301–307) © 2009 Blackwell Munksgaard

mRNA and protein. Mutated cell lines clustered into two areas, B and C; missense mutated cell lines fell into cluster B, and cell lines with mutations other than missense mutations (non-missense mutated cells) fell into cluster C. Thus, mutated cells were subdivided into two groups characterized by different imbalances in expression patterns between the transcript and protein levels because of mutations.

The *mdm2* mRNA levels also failed to correlate with either the *p53* mRNA (r = 0.256, P = 0.152) or protein (r = 0.1059, P = 0.409) levels. Differences in expression levels between wild-type and mutated cell lines were found only for *p53* mRNA, but not for p53 protein or *mdm2* mRNA. However, among the three groups of wild-type, missense mutated, and non-missense mutated cell lines, the association with *p53* mutational status was the highest for p53 protein levels, followed by *p53* mRNA levels, and then *mdm2* mRNA levels (P = 0.0033 vs. 0.0042 vs. 0.081, Kruskal–Wallis test).

Table 3 Comparison of total p53 protein concentration and the degree of p53 activation induced by Nutlin-3 in the various cell lines

		Nutlin-Induced p53 activation		
	p53 protein (ng/ml)[1]	DNA-binding capacity (induction fold)[2]	Phospho-p53^{ser15} (induction fold)[2]	Apoptosis (degree)[3]
Wild-type cells				
ST1	1.59	15.0	16.3	++
KOB	5.47	2.5	4.2	+
LM-Y1	3.82	3.9	6.1	+
OMT	5.85	2.8	19.8	+
MT2	2.58	3.5	8.9	+
HUt102	2.21	4.5	20.9	+
MOLt4	1.65	14.7	19.6	+
SuDHL	3.92	5.1	12.5	++
HS-Sultan	8.65	nt	nt	–
Mutant cells with missense				
KK1	5.23	2.2	0.8	+/–
Ramos	10.17	1.4	1.2	–
MT1s	1.17	10.7	11.8	+
SO4	15.00	2.4	1.5	–
Mutant cells without missense				
Jurkat	0.44	<0.1	<0.5	–
THP1	0.06	NC	NC	–
U937	0.26	NC	NC	–
HL60	0.07	NC	NC	–
K562	0.07	NC	NC	–

NC, no change in fold induction.
[1]The p53 protein concentration was displayed as pg/10 μg cell lysates.
[2]The degree of the DNA-binding and phospho-p53^{ser15} capacity was scored as induction fold relative to the measures before and after treatment with Nutlin-3.
[3]Apoptotic cells assessed as cells staining for annexin-V and propidium iodide (++, 50% or more; +, 10–50%; ±, 10% or less).

Analysis of p53 activation induced by Nutlin-3

To analyze, the activation of p53 aberrantly expressed in the cell lines, a transcription factor assay was performed as a marker of the DNA-binding capacity and the phosphorylation assay was performed to detect p53^{ser15}. These assays showed characteristic results specific for each group, classified according to the type of mutations, as summarized in Table 3. In wild-type cell lines, p53 was expressed at intermediate levels, and the DNA-binding and phosphorylation capacity of p53 were evident, leading to apoptosis after treatment with Nutlin-3. However, although missense mutated cell lines expressed high levels of p53 protein, the DNA-binding and phosphorylation capacities were poor and apoptotic induction varied, indicating that the quantity and function of missense mutated p53 were not associated. In non-missense mutated cell lines, p53 protein was rarely detected, and p53 activation and apoptosis were not induced.

Discussion

p53 mutations currently have the distinction of being the commonest mutations found in human cancers, including hematologic malignancies. *p53* is a tumor suppressor gene and inactivation of *p53* function is a causative event in oncogenesis.

This study analyzed *p53* mutational status in the entire ORF, and the types of mutations were related to the quantitative expression of *p53* mRNA and protein in 22 hematopoietic cell lines. The results showed that half of the cell lines harbored *p53* mutations and that the mutations occurred preferentially in arginine-encoding alleles of the *p53* codon 72 polymorphism. Notably, four of nine ATL-derived cell lines had carried p53 mutations on different sites with three missense and one silent. The p53 protein levels in mutated cells were not correlated with the levels of *p53* mRNA, and cells with missense mutations exclusively harbored over-expressed p53 proteins. Mutated p53 proteins, despite of over-expression, were defective for Nutlin-mediated activation and stabilization. These abnormalities in both the levels and functioning of the p53 protein depended on the type of mutations, and not solely on the presence of mutations.

The frequency of *p53* mutations found in these cell lines seems to be slightly higher than, or similar to, that found in primary hematologic malignancies, such as 39% in acute lymphoblastic leukemia, 44% in ATL, 32% in acute myelogenous leukemia, and 42% in chronic lymphocytic leukemia (16–18). Most mutations detected in this study were single nucleotide substitutions, being

© 2009 The Authors
Journal compilation **82** (301–307) © 2009 Blackwell Munksgaard

mainly missense mutations, followed by deletion, insertion, nonsense, and silent mutations. About 90% of the mutations were located from amino acids 102 to 292, which contains the DNA-binding domain. Consistent with results on the *p53* codon 72 polymorphism involving in the dominant-negative function and cancer risk (19, 20), *p53* mutations found in cell lines in this study occurred preferentially in the arginine-encoding alleles. In contrast, the allelic frequency in the wild-type cell lines was almost the same as in Japanese controls; 0.55 (Arg) vs. 0.45 (Pro) in this study, and 0.58 and 0.42 in Japanese controls. These *p53* mutational profiles of hematologic cell lines are similar to the pattern found in primary malignant solid tumors and hematologic malignancies reported in the database by Prokocimer *et al.* (18).

MDM2 mediates the ubiquitin-dependent degradation of p53, enhancing tumorigenic potential and resistance to apoptosis. Our data showed that the resistance to Nutlin-mediated apoptosis was basically associated with the presence and type of p53 mutations, although there existed several exceptional cases, such as HS-Sultan and MT1s (Table 3). This means that many complicated factors alternative to MDM2-p53 interaction, such as anti-apoptotic inhibitors, ATM, single polymorphic gene, and so on, may be involved in the Nutlin-induced apoptosis. A unique association between *p53* mutational status and *p53* mRNA and protein expression levels, quantified by real-time RT-PCR and Luminex methods, was also demonstrated in this study. The expression levels of *p53* mRNA in mutated cell lines were lower than in wild-type cell lines, indicating that *p53* mRNA quantification is useful for detecting the presence or absence of mutations. The present data on *p53* mRNA quantification were similar to those reported by Baumbush *et al.* (21), whose data showed that the expression levels of *p53* mRNA were highest in mutated tumors with missense mutations, followed by wild-type tumors, and then mutated tumors with nonsense and deletion mutations. Although the *p53* mRNA levels quantified by RT-PCR seem to show a marked variability, the aberrant expression of *p53* mRNA in mutated cell lines seemed to be consistent. Mutated cell lines with missense mutations over-expressed p53 protein despite having lower mRNA expression levels than in wild-type cell lines. Recent studies have shown that the p53 protein levels do not necessarily correlate with p53 mRNA at the transcript level, even in normal cells, because of the short half-life of the wild-type p53 protein (1). This study found that p53 over-expression was closely associated with missense mutations, but was not correlated with *p53* mRNA or *mdm2* mRNA expression levels. This finding suggests that structural alterations of the mutant protein modulated by missense mutations may be involved in the degradation of the protein, through post-translational modification (22–24). However, cell lines with non-missense mutations had neither detectable levels of *p53* mRNA nor protein. This is probably explained by impairment of the pretranslational stage. Overall, this unique association implies that *p53* mutations can affect the expression levels and functioning of the p53 protein.

In conclusion, the results of this study suggest that the frequency of *p53* mutations in hematopoietic cell lines is 50%. They also demonstrate that a unique association exists between the *p53* mutational status and the expression levels and functioning of its mRNA and protein, which depended not only on the presence or absence of mutations but also on the type of mutation. The characteristics observed in mutated cell lines could act as biomarkers to allow the better understanding of *p53*-associated tumor biology, and for screening for *p53* status in clinical settings.

Acknowledgements

This study was supported financially by a Japanese national grant, Kakenn, No. 17390165.

Author's contribution

SK designed this study, interpreted the data, and wrote the manuscript. AU, TT, DS, HH, and KY carried out molecular experiments, and KT and YY supplied and maintained cell lines and interpreted the data.

Competing interests

The authors declare that they have no competing interests.

References

1. Lain S, Lane DP. Tumor suppressor genes. In: Knowles M, Selby P, eds. *Introduction to the Cellular and Molecular Biology of Cancer*. Oxford: Oxford Press, 2005:135–55.
2. Poeta ML, Manola J, Goldwasser MA, *et al.* TP53 mutations and survivin in squamous-cell carcinoma of the head and neck. *N Eng J Med* 2007;**357**:2552–61.
3. Quon KC, Berns A. Haplo-insufficiency? Let me count the way. *Genes Dev* 2001;**2**:113–23.
4. Soussi T, Asselain B, Hamroun D, Kato S, Ishioka C, Claustres M, Beroud V. Meta-analysis of the *p53* mutation database for mutant *p53* biological activity reveals a methodological bias in mutation detection. *Clin Cancer Res* 2006;**12**:62–9.
5. Thomas M, Kalita A, Labrcque S, Pim D, Banks L, Matlashewski G. Two polymorphic variants of wild-type p53 differ biochemically and biologically. *Cell Mol Biol* 1999;**19**:1029–100.

© 2009 The Authors
Journal compilation **82** (301–307) © 2009 Blackwell Munksgaard

6. Concin N, Zeillinger C, Tong D, *et al.* Comparison of *p53* mutational status with mRNA and protein expression in a panel of 24 human breast carcinoma cell lines. *Breast Cancer Res Treat* 2003;**79**:37–46.
7. Lynch LC, Milner J. Loss of one *p53* allele results in four-fold reduction of *p53* mRNA and protein: a basis for *p53* haplo-insufficiency. *Oncogene* 2006;**25**:3463–70.
8. Russo A, Migliavacca M, Zanna I, *et al. p53* Mutations in L3-loop zinc-binding domain, DNA-ploidy, and S phase fraction are independent prognosis indicators in colorectal cancer: a prospective study with a five-year follow-up. *Cancer Epidemiol Biomarkers Prev* 2002;**11**:1322–31.
9. Anensen N, Haaland I, D'Santos C, Van Belle W, Gjertsen BT. Proteomics of p53 in diagnostics and therapy of acute myeloid leukemia. *Curr Pharm Biotechnol* 2006;**7**:199–207.
10. Renneville A, Roumier C, Biggio V, Nibourel O, Boissel N, Fenaux P, Preudhomme C. Cooperating gene mutations in acute myeloid leukemia: a review of the literature. *Leukemia* 2008;**22**:915–31.
11. Tawara M, Hogerzeil SJ, Yamada Y, *et al.* Impact of *p53* aberration on the progression of adult T-cell leukemia/lymphoma. *Cancer Lett* 2006;**234**:249–55.
12. Vassilev LT, Vu BT, Graves B, *et al.* In vivo activation of the p53 pathway b small-molecule antagonists of MDM2. *Science* 2004;**303**:844–8.
13. Yamada Y, Sugawara K, Hata T, *et al.* Interleukin-15 (IL-15) can replace the IL-2 signal in IL-2-dependent adult T-cell leukemia (ATL) cell lines: expression of IL-15 receptor alpha on ATL cells. *Blood* 1998;**91**:4265–72.
14. Untergasser A, Nijveen H, Rao X, Bisseling T, Geurts R, Leunissen LKM. Primer3Plus, an enhanced web interface to Primer3. *Nucleic Acids Res* 2007;**35**:71–74. web service issue, doi:10.1093/nar/gkm306
15. Hasegawa H, Yamada Y, Komiyama K, *et al.* Dihydroflavonol BB-1, an extract of natural plant Blumea balsamifera, abrogates TRAIL resistance in leukemia cells. *Blood* 2006;**107**:679–88.
16. Wada M, Bartram CR, Nakamura H, *et al.* Analysis of *p53* mutations in a large series of lymphoid hematologic malignancies of childhood. *Blood* 1993;**82**:3163–9.
17. Hollstein M, Rice K, Greenblatt MS, Soussi T, Fuchs R, Sorlie T, Hovig E, Smith-Sorensen B, Montesano B, Harris CC. Database of p53 gene somatic mutations in human tumors and cell lines. *Nucleic Acids Res* 1994;**22**:3551–5.
18. Prokocimer M, Unger R, Rennert HS, Rotter V, Rennert G. Pooled analysis of *p53* mutations in hematological malignancies. *Hum Mutat* 1998;**12**:4–18.
19. Nelson HH, Wilkojmen M, Marsit CJ, Kelsey KT. TP53 mutation, allelism and survival in non-small cell lung cancer. *Carcinogenesis* 2005;**26**:1770–3.
20. Yatabe Y, Konishi H, Mitsudome T, Nakamura S, Takahashi T. Topographical distributions of allelic loss in individual non-small cell lung cancers. *Am J Pathol* 2000;**157**:985–93.
21. Baumbusch LO, Myhre S, Langerod A, Bergamaschi A, Geisler SB, Lonning PE, Deppert W, Dornreiter I, Borresen-Dale AL. Expression of full-length p53 and its isoform delta-p53 in breast carcinomas in relation to mutation status and clinical parameters. *Mol Cancer* 2006;**5**:47 http://www.molecular-cancer.com/content/51/47.
22. Yins Y, Charles W, Stephenst M, Lucianis G, Fahraeuss R. *p53* stability and activity is regulated by Mdm2-mediated induction of alternative p53 translation products. *Nat Cell Biol* 2002;**4**:462–7.
23. Mills AA. *p53*: link to the past, bridge to the future. *Genes Dev* 2005;**19**:2091–9.
24. Walker DR, Bond JP, Tarone RE, Harris CC, Makalowski W, Boguski MS, Greenblatt MS. Evolutionary conservation and somatic mutation hotspot maps of *p53*: correlation with p53 protein structural and functional features. *Oncogene* 1999;**19**:211–8.

© 2009 The Authors
Journal compilation **82** (301–307) © 2009 Blackwell Munksgaard

Leukemia (2009) 23, 2090–2101
© 2009 Macmillan Publishers Limited All rights reserved 0887-6924/09 $32.00
www.nature.com/leu

ORIGINAL ARTICLE

Activation of p53 by Nutlin-3a, an antagonist of MDM2, induces apoptosis and cellular senescence in adult T-cell leukemia cells

H Hasegawa[1], Y Yamada[1], H Iha[2], K Tsukasaki[3], K Nagai[4], S Atogami[1], K Sugahara[1], K Tsuruda[1], A Ishizaki[1] and S Kamihira[1]

[1]*Department of Laboratory Medicine, Nagasaki University Graduate School of Biomedical Sciences, Nagasaki, Japan;* [2]*Department of Infectious Diseases, Faculty of Medicine, Oita University, Yufu, Oita, Japan;* [3]*Department of Hematology, Atomic Disease Institute, Nagasaki University Graduate School of Biomedical Sciences, Nagasaki, Japan and* [4]*Transfusion Service, Nagasaki University Hospital of Medicine and Dentistry, Nagasaki, Japan*

It has been reported that the induction of cellular senescence through p53 activation is an effective strategy in tumor regression. Unfortunately, however, tumors including adult T-cell leukemia/lymphoma (ATL) have disadvantages such as p53 mutations and a lack of $p16^{INK4a}$ and/or $p14^{ARF}$. In this study we characterized Nutlin-3a-induced cell death in 16 leukemia/lymphoma cell lines. Eight cell lines, including six ATL-related cell lines, had wild-type p53 and Nutlin-3a-activated p53, and the cell lines underwent apoptosis or cell-cycle arrest, whereas eight cell lines with mutated p53 were resistant. Interestingly, senescence-associated-β-galactosidase (SA-β-gal) staining revealed that only ATL-related cell lines with wild-type p53 showed cellular senescence, although they lack both $p16^{INK4a}$ and $p14^{ARF}$. These results indicate that cellular senescence is an important event in p53-dependent cell death in ATL cells and is inducible without $p16^{INK4a}$ and $p14^{ARF}$. Furthermore, knockdown of Tp53-induced glycolysis and apoptosis regulator (TIGAR), a novel target gene of p53, by small interfering RNA(siRNA) indicated its important role in the induction of cellular senescence. As many patients with ATL carry wild-type p53, our study suggests that p53 activation by Nutlin-3a is a promising strategy in ATL. We also found synergism with a combination of Nutlin-3a and tumor necrosis factor-related apoptosis-inducing ligand (TRAIL), suggesting the application of Nutlin-3a-based therapy to be broader than expected.
Leukemia (2009) **23,** 2090–2101; doi:10.1038/leu.2009.171; published online 27 August 2009
Keywords: p53; senescence; apoptosis; $p14^{ARF}$; adult T-cell leukemia; Nutlin

Introduction

DNA damage activates the tumor-suppressor protein, p53, as part of the surveillance mechanism.[1] Through the transcriptional activation or inactivation of target genes, p53 executes the appropriate physiological response, such as apoptosis, cell-cycle arrest or senescence.[2] To date, a number of target genes involved in p53-induced apoptosis have been identified, such as *BAX, NOXA, PUMA, PIG3* and *DR5*.[3,4] p53 can inhibit cell-cycle progression by initiating arrest at the G1, S or G2 phases. An inhibitor of cyclin-dependent kinase $p21^{WAF1/CIP1}$ (p21), GADD45α and 14-3-3σ have been implicated as major mediators of p53-induced growth arrest.[5] In addition, the recent discovery of a new target gene, C12orf5, also known as TP53-induced glycolysis, and an apoptosis regulator, Tp53-induced glycolysis and apoptosis regulator (TIGAR), revealed an unexpected function of p53 that regulates glucose metabolism and apoptosis.[6] Substantial evidence supports the idea that p53 can drive either apoptosis or cell-cycle arrest depending on which target genes it chooses to activate.[1,4] Meanwhile, a recent study showed that hematopoietic zinc-finger (Hzf) is induced by p53 and binds to its DNA-binding domain, resulting in the preferential transactivation of pro-arrest p53 target genes over its pro-apoptotic target genes.[7,8] These findings suggest that Hzf has an important role in regulating cell-fate decisions in response to genotoxic stress.

Cellular senescence is also an important mechanism in tumor suppression, which can be triggered by DNA damage or oncogene activation.[9] Cells entering cellular senescence are characterized by persistent cell-cycle arrest, a large flattened morphology, failure to replicate their DNA and enzymatic activity senescence-associated-β-galactosidase (SA-β-gal). The tumor suppressors $p16^{INK4a}$ (p16) and $p14^{ARF}$ (p14) have long been recognized as mediators of senescence, and research on oncogene-induced senescence has progressed rapidly; however, many questions remain regarding the programs and signals of cellular senescence.[10,11]

Adult T-cell leukemia/lymphoma (ATL) is a neoplasm of T-lymphocyte origin etiologically associated with human T-cell lymphotropic virus type 1(HTLV-1), and is known to be resistant to standard anticancer therapies.[12–14] HTLV-1 Tax has been shown to interfere with most DNA repair mechanisms, prevent cell-cycle arrest and apoptosis and contribute to the stepwise leukemic process leading to ATL.[15,16] Earlier studies using a p53-responsive reporter plasmid pG13-Luc and/or γ-irradiation have shown that Tax can repress the transcriptional activity of p53 in various transformed cell lines.[17–19] To date, several different mechanisms by which Tax inactivates p53 have been proposed, although the effects are indirect and complex.[20,21]

Mutations in the *p53* gene are found in about 50% of human cancers, and they abrogate DNA binding and the transactivation of p53.[22] Wild-type p53 protein is inactivated through binding to a specific E3 ubiquitin ligase, MDM2, which mediates the degradation of p53. Recently, a small antagonist of MDM2, Nutlin-3a, has been developed. Nutlin-3a binds MDM2 in the p53-binding pocket, activates the p53 pathway in human cancer cells with wild-type p53 and has shown promising results in an animal tumor model.[23,24] As mutated p53 proteins have been found in less than one-fourth of ATL cases and Tax expression is frequently lost in primary ATL cells, the activation of p53 by therapeutic drugs may become a promising approach to ATL therapy.[13,25]

In this study we analyze the potential therapeutic utility of Nutlin-3a in a number of ATL-related cell lines. Our experiments also provide new insights into the mechanism of cellular

Correspondence: Dr Y Yamada, Department of Laboratory Medicine, Nagasaki University Graduate School of Biomedical Sciences, 1-7-1 Sakamoto, Nagasaki City 852-8501, Japan.
E-mail: y-yamada@nagasaki-u.ac.jp
Received 12 May 2009; revised 20 July 2009; accepted 23 July 2009; published online 27 August 2009

senescence and the possibility of expanding Nutlin-3a-based cancer therapy.

Materials and methods

Cell lines

The ATL-derived cell lines, ST1, KOB, LM-Y1, KK1, SO4 and OMT, were established in our laboratory from the respective ATL patients.[26] These cell lines were maintained in RPMI 1640 medium supplemented with 10% fetal bovine serum and 0.5 U/ml of interleukin (IL-2) (kindly provided by Takeda Pharmaceutical Company, Ltd., Osaka, Japan). We also used the ATL-derived cell line MT1, HTLV-1-infected T-cell lines MT2[27] and HuT102,[28] human T-cell leukemia cell lines Jurkat and MOLT-4, human B lymphoblastoid cell line SKW6.4, Burkitt lymphoma cell line Ramos, transformed follicular lymphoma cell line SUDHL-4, acute myeloid leukemia cell line HL-60, monocytic leukemia cell lines THP-1 and U937 and erythromyeloblastoid cell line K562. These cell lines were maintained in RPMI 1640 medium supplemented with 10% fetal bovine serum.

Mutation analysis of p53

Total RNA from cell lines was isolated using ISOGEN (Wako, Osaka, Japan). After contaminating DNA was removed (Message Clean kit; GenHunter, Nashville, TN, USA), complementary DNA was constructed using the Thermoscript PCR with reverse transcription System (Invitrogen, Carlsbad, CA, USA) according to the manufacturer's protocol. Reverse transcriptase-PCR was performed to amplify the sequence targeting the open reading frame of p53 (GenBank accession number NM_000546) with the following primers: (forward) 5′-TCCGGGGACACTTTG CGTT-3′ and (reverse) 5′-AGGTGTGCGTCAGAAGCACC-3′. PCR products were then sequenced and analyzed using the BigDye Terminator v3.1 Cycle Sequencing kit (Applied Biosystems, Foster City, CA, USA) and an ABI-PRISM model 310 Genetic Analyzer (Applied Biosystems). All mutations were confirmed by sequencing in both directions. Additional primers for sequencing were as follows: (forward) 5′-TGCATTCTGGGA-CAGCCAAGT-3′ and 5′-CATCACACTGGAAGACTC-3′, and (reverse) 5′-CCAAGTCTGTGACTTGCACGTACT-3′ and 5′-GA GGAAGAGAATCTCCGCAAGAAAG-3′.

Deletion analysis of p14 *and* p16 *and quantitative PCR for human T-cell lymphotropic virus type 1 (HTLV-I) Tax*

As *p16* and *p14* share *exon 2* but have different open reading frames, loss of DNA in this region means the deletion of both proteins. Deletions of *p16* and *p14* were analyzed using *p16 exon 1-α* and *p14 exon 1-β* respectively. We designed specific sets of primers and TaqMan probes as follows: for *p16 exon 1-α*: 5′-GAGCAGCATGGAGCCTTC-3′ and 5′-CGTAACTATTCGGT GCGTTG-3′, TaqMan probe: 6FAM-CCGCACCTCTACCCGAC CC-TAMRA, for *p14 exon 1-β*: 5′-GCGCAGGTTCTTGGTGAC-3′ and 5′-CCTGAGTAGCATCAGCACGA-3′, TaqMan probe: 6FAM-TGTGAACCACGAAAACCCTCACTCG-TAMRA, for *INK4a/ARF exon 2*: 5′-ATTGAAAGAACCAGAGAGGC-3′ and 5′-ACGTTAA AAGGCAGGACATT-3′, TaqMan probe: 6FAM-ACCGAAGGTC CTACAGGGCCACAACT-TAMRA and for *β-globin*: 5′-CTTG AGGTTGTCCAGGTG-3′ and 5′-TGCTGGTGGTCTACCCTT-3′, TaqMan probe: 6FAM-GCCATGAGCCTTCACCTTAGGGTT G-TAMRA. Genomic DNA from cell lines was isolated using a QIAamp DNA Blood Mini Kit (Qiagen, Hilden, Germany) and subjected to a real-time quantitative PCR method based on TaqMan chemistry. PCRs were performed using Roche LC480 (Roche Diagnostics, Basel, Switzerland) with LightCycler 480 Probes Master mix (Roche Diagnostics) according to the manufacturer's directions. All data were normalized to the *β-globin* gene measured in the same samples. Samples with levels below the detection limit were considered to have homozygous deletions. Real-time quantitative PCR for HTLV-I Tax was performed as previously described.[29]

Chemicals and cell proliferation assay

Nutlin-3a (Alexis, San Diego, CA, USA), recombinant human soluble-TRAIL (Biomol Research Laboratories, Plymouth Meeting, PA, USA) and sodium butylate (Merck, Darmstadt, Germany) were used in this study. The cell proliferation assay (MTS assay) was performed using Cell Titer 96 AQueos Cell Proliferation Assay kit (Promega, Madison, WI, USA) in accordance with the manufacturer's instructions. Determination of the synergistic effect of combined treatment with Nutlin-3a and tumor necrosis factor-related apoptosis-inducing ligand (TRAIL) was achieved using isobolographic analysis, as described earlier.[30]

Flow cytometric detection of apoptosis, cell-cycle analysis and death receptors

Apoptosis and the cell cycle were examined using flow cytometry. To evaluate apoptotic changes, cells were stained simultaneously with Annexin-V and propidium iodide (Bender Medsystems, Vienna, Austria). Cell-cycle measurements based on DNA content were performed using a CycleTEST PLUS DNA reagent kit (BD Biosciences, San Jose, CA, USA). Cells were harvested after treatment and analyzed using a FACSCalibur flow cytometer and Cellquest software (BD Biosciences). The cell-surface expression of death receptors was examined by flow cytometer using DR5 (Alexis) or CD95 (BD Biosciences) monoclonal antibodies. Mouse IgG1 (DAKO, Kyoto, Japan) was used as a negative control.

Cellular senescence assay

For SA-β-gal staining, cells were harvested after treatment, and then placed on glass slides by cytospin centrifugation at 700 *g* for 5 min. Fixation of cells and staining for SA-β-gal in a humidified box kept at 37 °C overnight at pH 6.0 were performed using the Senescent Cells Staining kit (Sigma Chemicals, St Louis, MO, USA). The slides were washed three times in phosphate buffer solution and evaluated. May–Grünwald–Giemsa staining was also performed to distinguish between nuclear material and the cytoplasm. Cells were considered positive when the cytoplasm was stained with SA-β-gal.

Western blot analysis and antibodies

Whole cell lysates (20–40 μg) were prepared and western blotting was performed as described earlier.[31] Analysis was performed using antibodies to p53 (DO-1), MDM2 (Ab-1), PUMA, NOXA and PIG3 (Merck); caspase-3, BAX, Bcl-xL and p21 (Cell Signaling Technology, Beverly, MA, USA); TIGAR and Hzf (Abcam, Cambridge, MA, USA); GADD45α and p27 (Santa Cruz Biotechnology, Santa Cruz, CA, USA); Bcl-2 and 14-3-3σ (Upstate Biotechnology, Waltham, MA, USA); c-FLIP (Dave-2) (Alexis); survivin (R&D Systems Inc., Minneapolis, MN, USA); DEC-1 (Novus Biologicals, Littleton, CO, USA); DcR2 (Cayman

Chemical, Ann Arbor, MI, USA); and β-actin and α-tubulin (Sigma Chemicals). HTLV-1 Tax was detected by anti-Tax monoclonal antibodies from the National Institutes of Health AIDS Research Reference Reagent Program.[32]

Luminex protein analysis

Protein expression of total p53 and phospho-p53^{ser15} was measured using a bead multiplex system (BioSource International, Camarillo, CA, USA). Samples were incubated for 2 h at room temperature with anti-p53 or anti-phospho-p53^{ser15} beads in a 96-well plate. Detector antibodies were added to each well and incubated for 1 h, and the plate was read using Luminex100 IS instrument (Luminex, Austin, TX, USA). The concentrations of p53 and phospho-p53^{ser15} were determined using a standard curve assayed at the same time with known amounts of recombinant p53 and phospho-p53^{ser15}. This method permits a quantitative analysis of p53 protein or phospho-p53^{ser15}, which is considered difficult in western blot analysis.

p53-DNA binding enzyme-linked immunosorbent assay

The TransAM p53 Transcription Factor Assay kit (Active Motif, Carlsbad, CA, USA) was used following the manufacturer's protocol. Nuclear extracts from cells were prepared using a nuclear/cytosol fractionation kit (BioVision, San Diego, CA, USA) according to the manufacturer's protocol. Samples were diluted to 10 μg total protein with lysis buffer and applied to plates containing an immobilized oligonucleotide containing the p53 consensus binding site. After 1 h at room temperature, plates were washed and incubated with p53 antibody for another hour. After incubation with the secondary antibody, the developing solution was added, incubation was continued to allow color development and absorbance was read at 450 nm with a reference wavelength of 650 nm.

Transfection, luciferase assay and small interfering RNA (siRNA)

Transfection was performed with a Cell Line Nucleofector kit V or kit T and the Nucleofector system (Amaxa Biosystems, Cologne, Germany). The transfection program for ST1 (O-17), HuT102 (O-16), KOB (T-20) and KK1 cells (T-20) was determined so that high levels of transfection efficiency and cell viability could be achieved (data not shown). Cells were transfected with the luciferase reporter plasmid containing 13 copies of a p53 consensus binding site (pG13-Luc) and incubated with or without Nutlin-3a for 24 h.[20] Luciferase activity in 10 μg cell lysate was measured using luciferase assay reagents (Promega) according to the manufacturer's instructions in a TD-20/20 luminometer (Turner Designs, Sunnyvale, CA, USA). Each experiment was carried out in triplicate. siRNA of p21 (Silencer Validated siRNA no. 1621), TIGAR (Silencer Select siRNA no. 32679) and control siRNA (Silencer Negative Control no. 1) were purchased from Applied Biosystems. Each siRNA was transfected at a final concentration of 20 nM. At 24 h after transfection, cells were used for experimentation.

Results

Mutations of p53 *and deletions of* p14 *and* p16

We first analyzed the p53 status of 16 hematological cell lines, including 9 ATL-related cell lines, and found that 8 had wild-type p53 and 8 had mutated p53 (Table 1). ST1, KOB and OMT had single nucleotide polymorphisms at codon 72, which is the most extensively studied polymorphism in p53.[22] Consistent with previous reports, there was no mutation in p53 of HuT102, MT2, SUDHL-4 and MOLT-4 cells.[33–35] Mutations detected in Ramos and Jurkat, deletions in HL60 and an insertion in K562 cells were all in accordance with earlier reports[34,36–38] or the data from the International Agency for Research on Cancer (http://www-p53.iarc.fr/). Accordingly, six of nine ATL-related

Table 1 Mutations of p53 and deletions of *p14* and/or *p16*

Cell line	*Origin*	*Exon*	*Codon*	*WT codon*	*Mutant codon*	*Effect*	*p53 Status*	p16^{INK4a}/p14^{ARF}	*HTLV-I-Tax mRNA*
ST1	ATL	4	72	CCC	CGC	Missense (SNP)	WT	del/del	0.4
KOB	ATL	4	72	CCC	CGC	Missense (SNP)	WT	del/del	542
LM-Y1	ATL	4	36	CCG	CCA	Silent	WT	del/del	1741
MT1	ATL	5	176	TCG	TAC	Missense	MUT	del/del	17.5
SO4	ATL	6	223	CCT	CAT	Missense	MUT	del/del	0.2
KK1	ATL	3	31	GTT	ATT	Missense	MUT	del/del	0.03
		5	152	CCG	CTG	Missense			
OMT	HTLV-I-infected T-cell	4	72	CCC	CGC	Missense (SNP)	WT	del/del	971
HuT102	HTLV-I-infected T-cell						WT		2381
MT2	HTLV-I-infected T-cell						WT		9331
MOLT-4	T-cell leukemia						WT	del/del	ND
Jurkat	T-cell leukemia	4	125	ACG	ACA	Silent	MUT	del/del	0
		6	196	CGA	TGA	Nonsense			
SUDHL-4	B-cell lymphoma						WT	del/	ND
Ramos	B-cell lymphoma	7	254	ATC	GAC	Missense	MUT		ND
U937	Monocytic leukemia	4	105	GGC	AGC	Missense	MUT	del/del	ND
		4	125	ACG	ACA	Silent			
		6	196	CGA	TGA	Nonsense			
K562	Erythroblastic leukemia	4	72	CCC	CGC	Missense (SNP)	MUT	del/del	ND
		5	136			Ins 1			
HL60	Myeloid leukemia	Gross deletion					MUT		ND

Abbreviations: ATL, adult T-cell leukemia/lymphoma; blank column, intact; del, deletion; HTLV-1, human T-cell lymphotropic virus type 1; ins, insertion; MUT, mutation; ND, not determined; SNP, single nucleotide polymorphism; WT, wild type.
The p53 status was determined using direct sequence targeting of the open reading frame, after RNA isolation, complementary DNA synthesis and reverse transcriptase-PCR amplification (GenBank accession number NM_000546). Deletions of *p14* and *p16* were determined using genomic DNA by the real-time quantitative PCR method based on TaqMan chemistry (GenBank accession number AF527803). Quantitative analysis of HTLV-1-Tax mRNA expression was also performed.

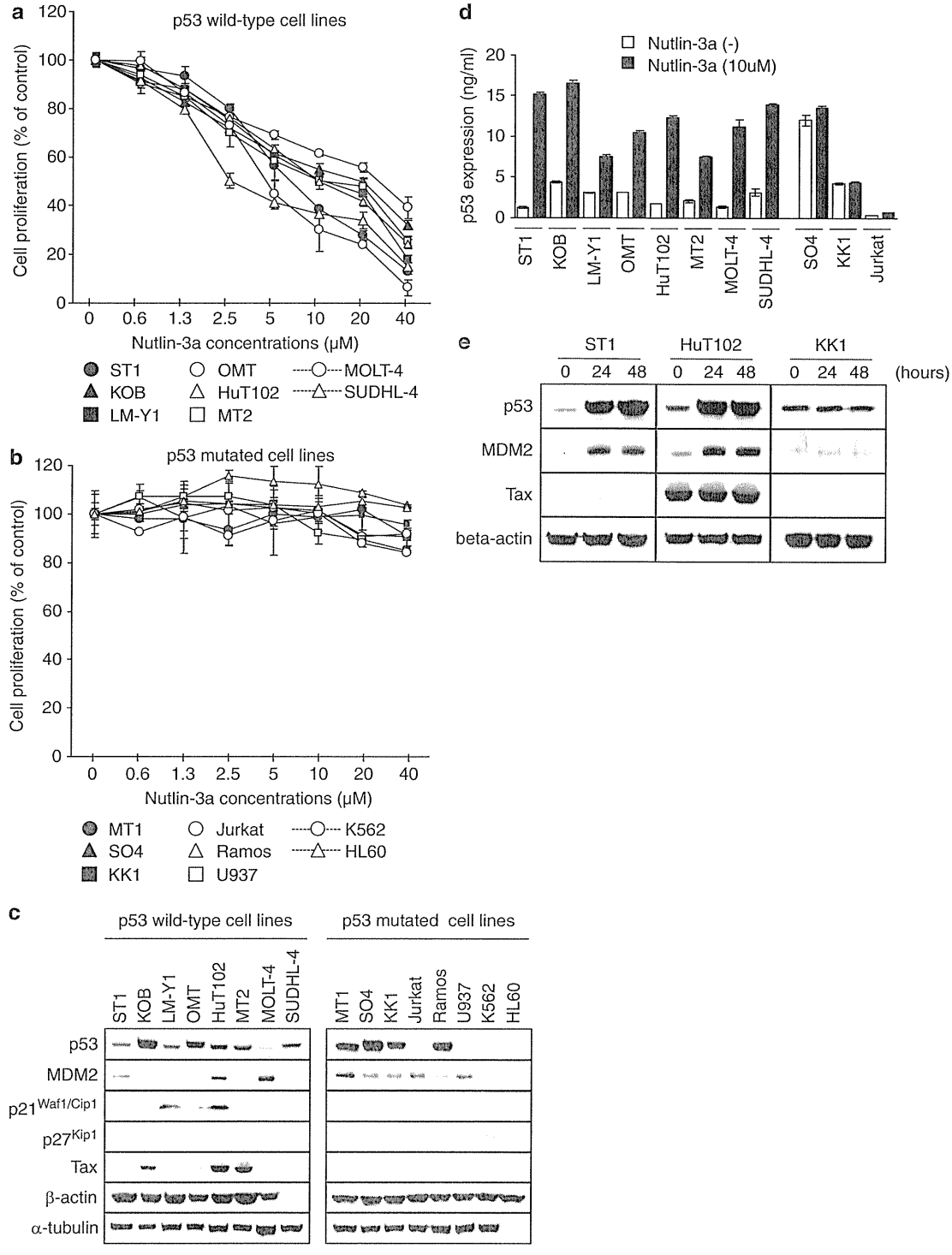

Figure 1 Sensitivity of hematological cell lines to Nutlin-3a and accumulation of p53 protein. (**a**, **b**) Cells ($5-7 \times 10^5$/ml) were cultured for 48 h with the indicated concentrations of Nutlin-3a, and cell proliferation (percentage against control cells) was evaluated using MTS assay. All experiments were performed in triplicate and the results are expressed as mean ± s.d. (**c**) Whole cell lysate (40 μg) was prepared and the basal expression levels of p53-related proteins were detected using western blot analysis. (**d**, **e**) Cells were cultured with or without 10 μM Nutlin-3a for 24 h or the indicated period. (**d**) About 10 μg cell lysate was prepared and Luminex analysis was performed to evaluate the accumulation of p53 protein. Experiments were performed in duplicate and the results are expressed as mean ± s.d. (**e**) Whole cell lysate (20 μg) was prepared and the expression levels of p53-related proteins were detected using western blot analysis.

cell lines carried wild-type p53 in our analysis. The results of deletion analysis of *p16* and *p14* genes are summarized in Table 1. Deletions of both *p16* and *p14* occurred in all ATL-derived cell lines, and 11 cell lines lacked both, irrespective of their p53 status.

Nutlin-3a induces cell-growth inhibition and accumulation of p53

We next examined the effect of Nutlin-3a on the growth of the 16 cell lines. All eight cell lines with wild-type p53 showed apparent growth inhibition following treatment with Nutlin-3a, but the eight cell lines with mutated p53 were resistant (Figures 1a and b). As Nutlin-3a is expected to stabilize and activate p53 protein, we first examined the basal expression levels of p53-related proteins by western blot analysis (Figure 1c). Among p53 wild-type cell lines, ATL-related cell lines had elevated basal levels of p53 and some cells also had detectable levels of p21, in agreement with earlier reports.[33,39,40] Four p53-mutated cell lines showed strong expression of p53, probably because of mutations, and the others showed almost no band, consistent with the fact that they have deletions or nonsense mutations (Table 1). More important, these results were in accordance with those of Luminex analysis (Figure 1d). Although KOB, LM-Y1 and K562 showed a faint expression of p27, other cell lines did not express detectable levels of p27. HTLV-1 Tax protein was detected in HuT102, MT2, OMT and KOB, which is coincident with the results of mRNA expression (Table 1). In Luminex analysis, p53 wild-type cell lines showed a 4- to 12-fold increase in p53 expression after 24-h exposure to Nutlin-3a as a result of the inhibition of p53 degradation, which was not observed in p53-mutated cell lines (Figure 1d). Furthermore, time-dependent accumulation of p53 and MDM2 was clearly detected using western blot analysis (Figure 1e and data not shown). Meanwhile, there was no change in the expression of HTLV-1 Tax by Nutlin-3a treatment (Figure 1e).

Activation of p53 by Nutlin-3a in adult T-cell leukemia/lymphoma (ATL)-related cell lines

In addition to the accumulation of p53 protein, we further evaluated transcriptional activities of p53 from various perspectives. We first analyzed the level of DNA-binding activity of p53 using enzyme-linked immunosorbent assay. When cells were treated with Nutlin-3a, all p53 wild-type cells showed higher activities than positive control cells (Figure 2a). Next, we transfected ST1, HuT102, KOB and KK1 cells with a luciferase reporter plasmid, pG13-Luc, treated with or without Nutlin-3a, and performed a luciferase assay. As a result, fold inductions of luciferase activities were observed in a dose-dependent manner and showed maximum activities with 5 μM Nutlin-3a in ST1 and HuT102 cells, whereas KK1 cells with mutated p53 showed no change (Figure 2b). Luminex analysis revealed that Nutlin-3a caused obvious phosphorylation of p53, a 4- to 20-fold increase, in all p53 wild-type cell lines, which had not occurred in KK1 cells (Figure 2c). These results indicate that Nutlin-3a causes the accumulation, increase of transcriptional activity and phosphorylation of p53 in ATL-related cell lines with endogenous wild-type p53.

Nutlin-3a causes apoptosis in p53 wild-type cells

To clarify the details of Nutlin-3a-induced cell death, we performed Annexin-V/propidium iodide staining in p53

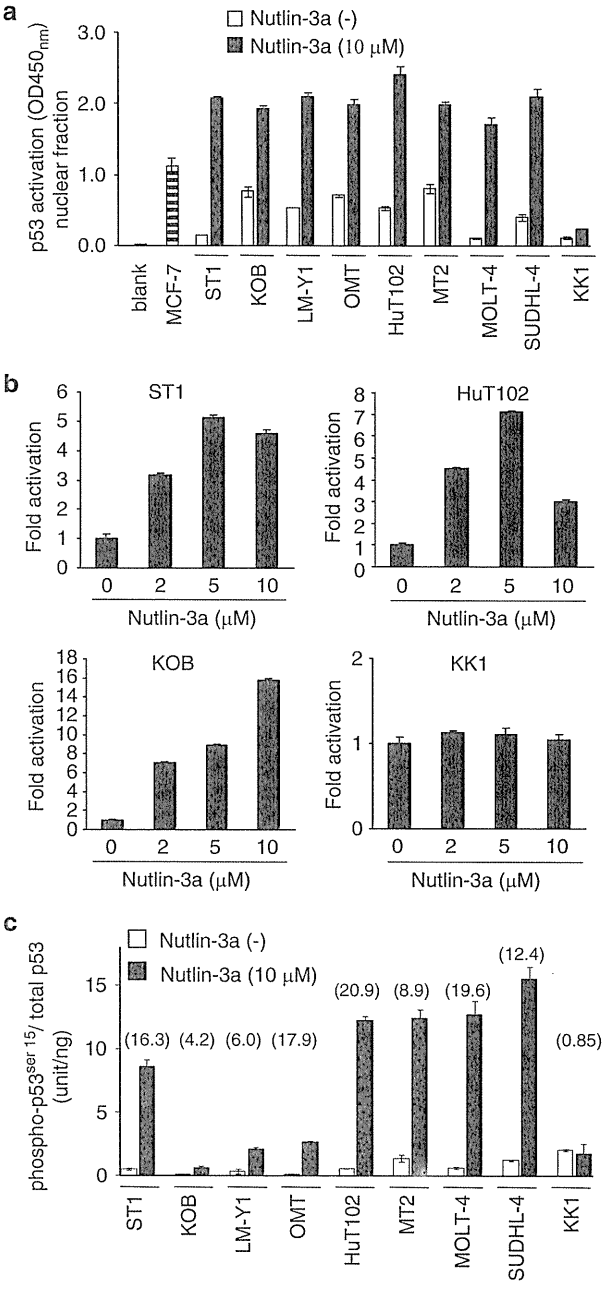

Figure 2 Transcriptional activation of p53 by Nutlin-3a treatment. Cells were treated with or without the indicated concentrations of Nutlin-3a for 24 h. After cells were harvested, enzyme-linked immunosorbent assay (ELISA), luciferase assay and Luminex analysis were performed. KK1 (p53 mutant) cells were used as an accumulation-negative control. (**a**) Nuclear extract from H_2O_2-treated MCF-7 cells contained in the kit was used as a positive control. About 10 μg nuclear extract was used, experiments were performed in duplicate and results are expressed as mean ± s.d. (**b**) For the luciferase assay, cells were co-transfected with 0.1 μg pG13-Luc, incubated for 12 h and treated with or without Nutlin-3a for 24 h. Experiments were performed in triplicate and results are expressed as the mean ± s.d. The level of activation (fold induction) was obtained by setting the value without Nutlin-3a as 1.0. (**c**) About 10 μg whole cell lysate was prepared, experiments were performed in duplicate and results are expressed as mean ± s.d. Fold induction was also obtained by setting the value without Nutlin-3a as 1.0 and is indicated on the graph.

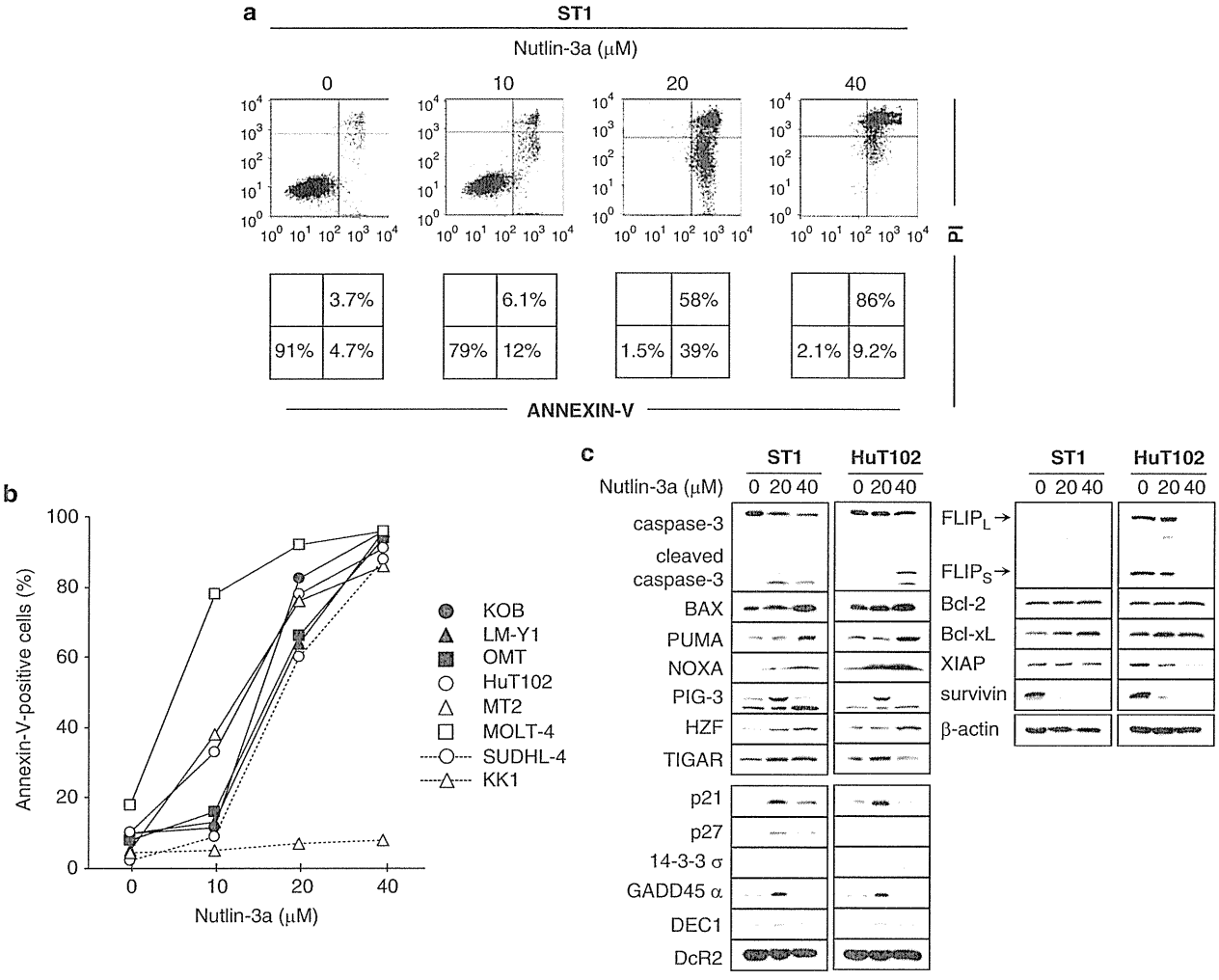

Figure 3 Analysis of molecules in Nutlin-3a-induced apoptosis. Cells were treated with or without the indicated concentrations of Nutlin-3a for 24 h. After cells were harvested, flow cytometric analyses by Annexin-V/ propidium iodide (PI) staining (**a**, **b**) and western blot analysis (**c**) were performed.

wild-type cell lines. We found weak apoptotic changes with 10 μM Nutlin-3a and less than 30% of cells became positive for Annexin-V, except MOLT-4 cells, which showed apparent apoptosis (Figures 3a and b). In contrast, with more than 20 μM Nutlin-3a, all p53 wild-type cell lines showed rapid apoptosis and almost no living cell fraction was observed by Annexin-V/propidium iodide staining. These results suggest that Nutlin-3a eventually causes apoptosis in p53 wild-type cell lines in a dose-dependent manner. We then performed western blot analysis of key molecules of the p53 pathway. In addition to cleaved forms of caspase-3, we found dose-dependent increase of BAX, PUMA, NOXA and Hzf, no change of Bcl-2 and dose-dependent decrease of XIAP and survivin (Figure 3c).

Nutlin-3a induces cellular senescence followed by cell-cycle arrest in p53 wild-type cells

Despite weak apoptotic changes, cell growth of p53 wild-type cell lines was significantly depressed by Nutlin-3a at a concentration of 10 μM. To clarify this discordance, we performed cell cycle analysis. When cells were treated with 10 μM Nutlin-3a for 24 h, these cells showed significant cell-cycle arrest in the G1 phase instead of apoptosis. The G1 cell population increased from 63 to 78% in ST1 and from 68 to 92% in HuT102 (Figure 4a). Similar results were observed in the other p53 wild-type cell lines (Figure 4b). Although it has been reported that p53 has a central role in the induction of cellular senescence, Nutlin-3a-induced cellular senescence has not been reported in leukemia cells.[41,42] We thus performed SA-β-gal staining as a marker of cellular senescence after incubation with 10 μM Nutlin-3a for 72 h. Five of eight p53 wild-type cell lines (ST1, HuT102, MT2, OMT and KOB) were clearly stained by SA-β-gal and all were ATL-related cell lines (Figure 4c and data not shown). No non-ATL cell lines became positive for SA-β-gal staining. In contrast, after treatment with 1 mM sodium butylate, a well-known senescence inducer, all cell lines examined, including those with mutant p53 (SO4 and K562), became positive for SA-β-gal staining (data not shown). Among five SA-β-gal-positive cell lines, three lacked both p16 and p14 (Table 1), suggesting that these cells underwent p53-dependent cellular senescence without the participation of p16 and/or p14. We further analyzed whether removal of Nutlin-3a alters cell fate, senescence or cell proliferation. To this purpose, p53 wild-type ATL cell lines were cultured with Nutlin-3a for 72 h to